NASA TECHNICAL NOTE

NASA TN D-2376

NASA TN D-2376

SUPERSONIC LATERAL-DIRECTIONAL STABILITY CHARACTERISTICS OF A 45° SWEPT WING-BODY-TAIL MODEL WITH VARIOUS BODY CROSS-SECTIONAL SHAPES

by Dennis E. Fuller and James F. Campbell

Langley Research Center
Langley Station, Hampton, Va.

NATIONAL AERONAUTICS AND SPACE ADMINISTRATION • WASHINGTON, D. C. • AUGUST 1964

SUPERSONIC LATERAL-DIRECTIONAL STABILITY CHARACTERISTICS OF A 45° SWEPT WING-BODY-TAIL MODEL WITH VARIOUS BODY CROSS-SECTIONAL SHAPES

By Dennis E. Fuller and James F. Campbell

Langley Research Center
Langley Station, Hampton, Va.

NATIONAL AERONAUTICS AND SPACE ADMINISTRATION

For sale by the Office of Technical Services, Department of Commerce,
Washington, D.C. 20230 -- Price $1.25

SUPERSONIC LATERAL-DIRECTIONAL STABILITY CHARACTERISTICS OF A 45° SWEPT WING-BODY-TAIL MODEL WITH VARIOUS BODY CROSS-SECTIONAL SHAPES

By Dennis E. Fuller and James F. Campbell
Langley Research Center

SUMMARY

An investigation has been made in the Langley 4- by 4-foot supersonic pressure tunnel to determine the lateral, directional, and longitudinal stability characteristics of a 45° swept wing-body-tail model having various body cross-sectional shapes. The cross-sectional shapes tested include a circle, an ellipse, a flat-bottom teardrop, an upright triangle, and an inverted triangle. Tests were performed at angles of attack of about -4° to 22°, at angles of sideslip from about -4° to 8°, at Mach numbers of 1.41 and 2.20, and at a Reynolds number per foot of 3.0×10^6.

The results indicate that the directional stability, particularly for high angles of attack, was found to be dependent on body cross-sectional shape. A circular fuselage generally indicates the least effects of angle of attack on the lateral-directional stability characteristics of any of the body shapes tested.

INTRODUCTION

There is a continuing problem of providing adequate lateral and directional stability for aircraft operating in the supersonic speed range. Previous papers, such as references 1 and 2, have described some of the sources of this problem and pointed out some of the factors that affect the stability at supersonic speeds. However, there is still a general lack of information in the supersonic speed range concerning the effects of various design variables on the static stability characteristics.

Some effort has been expended to determine the effect of body cross-sectional shape on the longitudinal stability and performance characteristics of bodies, wing-bodies, and aircraft (refs. 3, 4, and 5), but these studies have not included the lateral and directional stability characteristics. Accordingly, an investigation has been undertaken to determine the effect of

some basic fuselage shapes on the lateral and directional stability characteristics and on the vertical-tail effectiveness of wing-body-tail configurations at supersonic speeds. The cross-sectional shapes of the bodies included a circle, an ellipse, a flat-bottom teardrop, an upright triangle, and an inverted triangle. The wing and vertical tail for all of the bodies were the same. Tests to obtain the longitudinal characteristics of the various configurations were also included.

The tests were performed in the Langley 4- by 4-foot supersonic pressure tunnel at Mach numbers of 1.41 and 2.20, at angles of attack from about -4° to 22°, and angles of sideslip from about -4° to 8°. The test Reynolds number was 3.0×10^6 per foot.

SYMBOLS

The lateral force and moment data are referred to the body axis system and the longitudinal force and moment data are referred to the stability axis system. The reference center of moments was located at the 45.4-percent station of the fuselage. The symbols used are defined as follows:

a' semiminor axis

b' semimajor axis

b wing span, 24.00 in.

$\bar{c}$ wing mean geometric chord, 6.89 in.

C_D drag coefficient, $\frac{\text{Drag}}{qS_w}$

C_L lift coefficient, $\frac{\text{Lift}}{qS_w}$

C_m pitching-moment coefficient, $\frac{\text{Pitching moment}}{qS_w\bar{c}}$

C_l rolling-moment coefficient, $\frac{\text{Rolling moment}}{qS_wb}$

$$C_{l_\beta} = \frac{\Delta C_l}{\Delta \beta}$$

$$\Delta C_{l_\beta} = \left(C_{l_\beta}\right)_{\text{tail-on or wing-on}} - \left(C_{l_\beta}\right)_{\text{tail-off or wing-off}}$$

C_n yawing-moment coefficient, $\frac{\text{Yawing moment}}{qS_w b}$

$$C_{n_\beta} = \frac{\Delta C_n}{\Delta \beta}$$

$$\Delta C_{n_\beta} = \left(C_{n_\beta}\right)_{\text{tail-on or wing-on}} - \left(C_{n_\beta}\right)_{\text{tail-off or wing-off}}$$

C_Y side-force coefficient, $\frac{\text{Side force}}{qS_w}$

$$C_{Y_\beta} = \frac{\Delta C_Y}{\Delta \beta}$$

$$\Delta C_{Y_\beta} = \left(C_{Y_\beta}\right)_{\text{tail-on or wing-on}} - \left(C_{Y_\beta}\right)_{\text{tail-off or wing-off}}$$

L/D lift-drag ratio

M free-stream Mach number

q free-stream dynamic pressure

r radius

S_w reference wing area, 1.0 sq ft

x distance from nose, rearward

y distance from model center line, downward

α angle of attack, deg

β angle of sideslip, deg

APPARATUS AND TESTS

Model

Drawings of the model are presented in figure 1. Body cross-sectional areas and lateral areas are presented in table I and body nose coordinates are presented in table II. The wing had 45° sweepback of the quarter-chord line, an aspect ratio of 4, a taper ratio of 0.2 and NACA 65A004 airfoil sections in the streamwise direction. The vertical tail had a hexagonal section with 42° sweepback of the leading edge. The wing and vertical tail were affixed to a

steel core over which the various body shapes were fitted. Hence, for some of the body shapes, there are geometric variations in the exposed vertical-tail area and the vertical location of the wing relative to the body. The various body shapes were constructed of wood with a fiber-glass surface with the exception of the circle which had a stainless-steel nose.

TABLE I.- BODY CROSS-SECTIONAL AND LATERAL AREAS

Body shape	Cross-sectional area, sq in.	Lateral area, sq ft
Circle	9.621	0.856
Ellipse	14.432	1.287
Flat-bottom teardrop	13.022	1.064
Inverted and upright triangle	14.496	1.086

Tunnel

Tests were conducted in the Langley 4- by 4-foot supersonic pressure tunnel which is a continuous-flow tunnel with variable-pressure capability. The nozzle leading to the test section is symmetrical and may be manually changed to provide Mach numbers from about 1.4 to 2.2.

Test Conditions

The tests were performed at the following conditions:

Mach number	Stagnation temperature, ^{o}F	Stagnation pressure, lb/sq in. abs	Reynolds number, per ft
1.41	110	10.3	3.0×10^{6}
2.20	110	13.2	3.0×10^{6}

The stagnation dewpoint was maintained at -30^{o} F in order to avoid condensation effects. Tests were performed through an angle-of-attack range from about -4^{o} to 22^{o} and through a sideslip angle range from about -4^{o} to 8^{o}. In order to obtain turbulent flow over the model, a 1/16-inch-wide strip of No. 60 carborundum grains was affixed around the body one-half inch from the nose and on the wing and tail one-half inch from the leading edge in a streamwise direction.

TABLE II.- BODY NOSE COORDINATES

Circle	
x, in.	y, in.
0.000	0.000
.500	.143
1.000	.278
1.500	.408
2.000	.532
3.000	.761
4.000	.965
5.000	1.145
6.125	1.319
7.125	1.448
8.125	1.550
9.125	1.639
10.125	1.698
11.125	1.735
12.250	1.750

Ellipse		
x, in.	a', in.	b', in.
0.000	0.000	0.000
.500	.143	.194
1.000	.278	.417
1.500	.408	.612
2.000	.532	.798
3.000	.761	1.142
4.000	.965	1.448
5.000	1.145	1.718
6.125	1.319	1.979
7.125	1.448	2.172
8.125	1.550	2.325
9.125	1.639	2.459
10.125	1.698	2.547
11.125	1.735	2.603
12.250	1.750	2.625

Flat-bottom teardrop			
x, in.	a', in. (*)	b', in.	r, in.
0.000	0.000	0.000	0.000
.500	.143	.215	.070
1.000	.278	.417	.137
1.500	.408	.612	.201
2.000	.532	.798	.262
3.000	.761	1.142	.375
4.000	.965	1.448	.475
5.000	1.145	1.718	.564
6.125	1.319	1.979	.650
7.125	1.448	2.172	.722
8.125	1.550	2.325	.763
9.125	1.639	2.459	.807
10.125	1.698	2.547	.836
11.125	1.735	2.603	.855
12.250	1.750	2.625	.862

*a' = y.

Triangle, upright and inverted		
x, in.	y, in.	r, in.
0.000	0.000	0.000
.500	.143	.064
1.000	.278	.137
1.500	.408	.201
2.000	.532	.262
3.000	.761	.375
4.000	.965	.475
5.000	1.145	.564
6.125	1.319	.650
7.125	1.448	.722
8.125	1.550	.763
9.125	1.639	.807
10.125	1.698	.836
11.125	1.735	.855
12.250	1.750	.862

Measurements

Aerodynamic forces and moments were measured by means of a six-component electrical strain-gage balance housed within the model. The balance, in turn, was rigidly fastened to a sting support and thence to the tunnel support system. The balance-chamber pressure was measured by means of a single static orifice in the balance cavity of each model for all test conditions.

Accuracy

The accuracy of the measured quantities, based on calibrations and repeatability of data is estimated to be within the following limits:

C_D	±0.0002
C_l	±0.0001
C_L	±0.002
C_n	±0.0002
C_m	±0.0004
C_Y	±0.001
α, deg	±0.10
β, deg	±0.10
M	±0.01

Corrections

Angles of attack and sideslip were corrected for deflection of the balance and sting support as a result of aerodynamic loads. The drag data were adjusted to correspond to free-stream static conditions in the balance chamber.

PRESENTATION OF RESULTS

The results of the investigation are presented in the following figures:

	Figure
Typical aerodynamic characteristics in sideslip. Wing on; M = 1.41	2
Typical aerodynamic characteristics in sideslip. Wing on; M = 2.20	3
Variation of sideslip parameters with angle of attack for the circular fuselage. Wing on; M = 1.41 and 2.20	4
Variation of sideslip parameters with angle of attack for the flat-bottom teardrop fuselage. Wing-on; M = 1.41 and 2.20	5
Variation of sideslip parameters with angle of attack for the elliptical fuselage. Wing on; M = 1.41 and 2.20	6

RESULTS AND DISCUSSION

Basic aerodynamic characteristics in sideslip for the circular and the two triangular body configurations are presented in figures 2 and 3 for angles of attack of about 0°, 11°, and 16°. These figures are presented primarily to indicate the linearity of the data since the sideslip parameters presented herein were obtained from incremental results of tests made through the angle-of-attack range at sideslip angles of about 0° and 4°. The sideslip coefficients are essentially linear with sideslip angle with the exception of some of the results at an angle of attack of about 16° wherein the nonlinearity will cause some error in the absolute values of the sideslip parameters presented.

The variation of the sideslip parameters with angle of attack for all the configurations are presented in figures 4 to 8 and the tail contributions to the sideslip derivatives are presented in figure 9. A direct comparison of the results cannot be made since the individual models represent separate configurations that differ not only in cross-sectional shape and area (see table I) but also in exposed tail and wing area, relative wing height, and lateral area.

As the angle of attack is increased the variation of the sideslip derivatives becomes involved and is partly dependent on the cross-flow pattern about the bodies and the formation of wake patterns from the forebody and wing-body juncture. In general, the circular body, which is the only shape that consistently provides a symmetrical cross-flow pattern at combined angles of attack and sideslip, indicates the least variation of sideslip derivatives and tail contribution with angle of attack. (See figs. 4 and 9.)

The only configurations having substantial differences in cross section while maintaining the same volume and area distribution are those with the upright and inverted triangular sections. For the purpose of comparison, the results for these configurations with the wing on are presented in figure 7 and with the wing removed in figure 8. The results indicate that differences occur in the sideslip characteristics for the two body shapes. Near $\alpha = 0^\circ$, for example, the directional stability, with wing on and wing off, is greater with the inverted triangle fuselage than with the upright triangle fuselage, presumably because the vertical tail on the inverted triangle fuselage has a

slightly greater exposed area. However, with increasing angle of attack, the upright triangle fuselage indicates less deterioration in C_{n_β} than the inverted triangle fuselage, and at high angles of attack results in a substantially higher level of directional stability. This higher level of stability is influenced both by the tail contribution and the tail-off stability characteristics, and a comparison of the wing-on and wing-off results indicate these factors are also influenced by the wing. (See figs. 7, 8, and 10.) Although it is not possible to isolate completely the causes of these results from total force and moment measurements, the variations in the results do point out a strong effect of body cross section that adds to the complexity of the lateral-directional stability characteristics and indicate some of the factors that must be considered in attempting to solve the lateral-directional stability problems.

The aerodynamic characteristics in pitch for the test configurations are presented in figure 11. Since some of the bodies were of different volumes as well as cross-sectional areas, no attempt has been made to analyze these data.

SUMMARY OF RESULTS

Tests to determine the static lateral-directional stability characteristics at Mach numbers of 1.41 and 2.20 of configurations having various body cross-sectional shapes indicated the following results:

1. The directional stability, particularly for high angles of attack, was found to be dependent on body cross-sectional shape.

2. A circular fuselage generally indicated the least effects of angle of attack on the lateral-directional stability characteristics of any of the body shapes investigated.

Langley Research Center,
National Aeronautics and Space Administration,
Langley Station, Hampton, Va., April 18, 1964.

REFERENCES

1. Spearman, M. Leroy: Some Factors Affecting the Static Longitudinal and Directional Stability Characteristics of Supersonic Aircraft Configurations. NACA RM L57E24a, 1957.

2. Spearman, M. Leroy, and Henderson, Arthur, Jr.: Some Effects of Aircraft Configuration on Static Longitudinal and Directional Stability Characteristics at Supersonic Mach Numbers Below 3. NACA RM L55L15a, 1956.

3. Jorgensen, Leland H.: Inclined Bodies of Various Cross Sections at Supersonic Speeds. NASA MEMO 10-3-58A, 1958.

4. Carlson, Harry W., and Gapcynski, John P.: An Experimental Investigation at a Mach Number of 2.01 of the Effects of Body Cross-Section Shape on the Aerodynamic Characteristics of Bodies and Wing-Body Combinations. NACA RM L55E23, 1955.

5. Fuller, Dennis E., Shaw, David S., and Wassum, Donald L.: Effect of Cross-Section Shape on the Aerodynamic Characteristics of Bodies at Mach Numbers From 2.50 to 4.63. NASA TN D-1620, 1963.

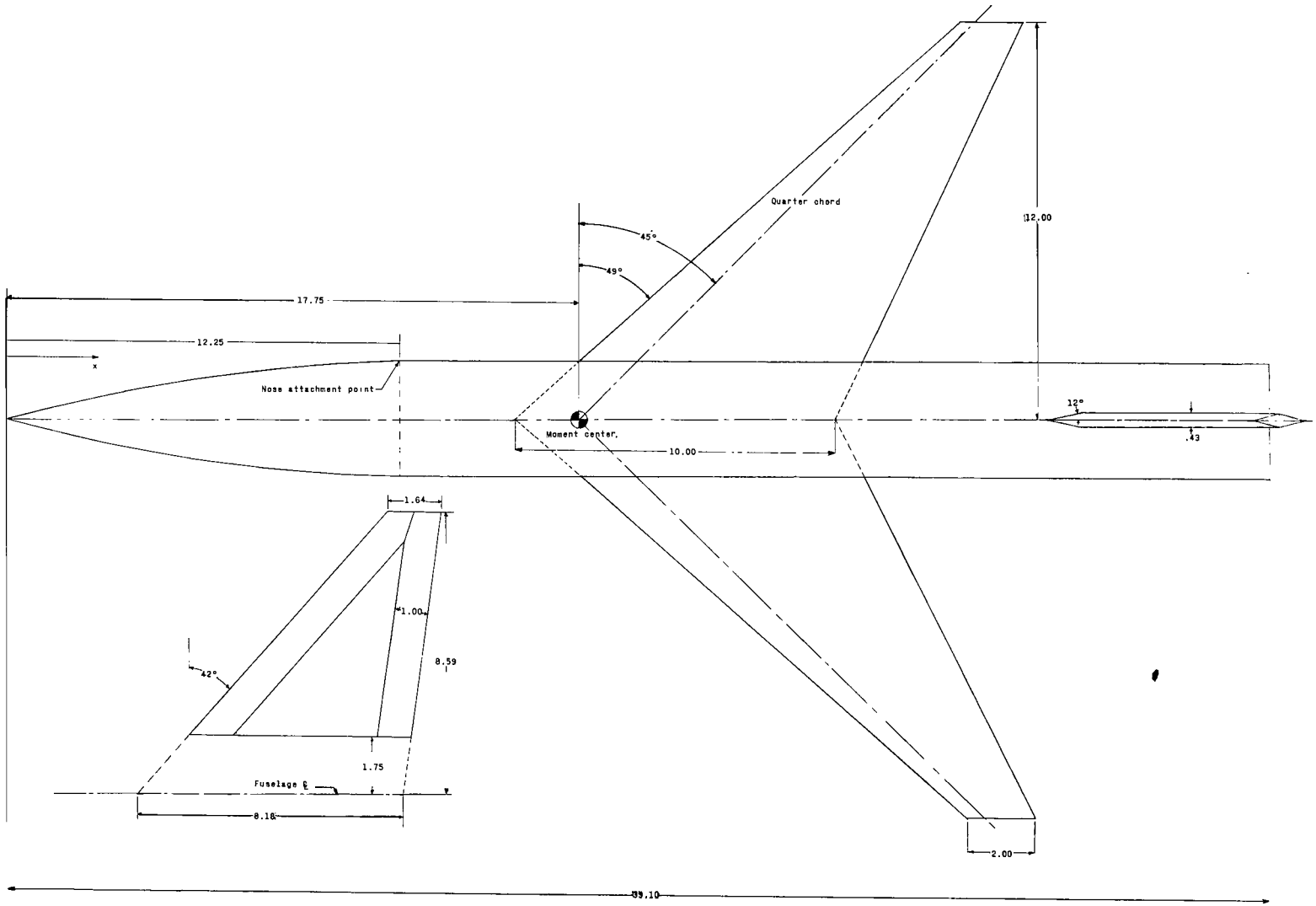

(a) Model with circular fuselage and vertical tail.

Figure 1.- Model drawings. All dimensions are in inches unless otherwise noted.

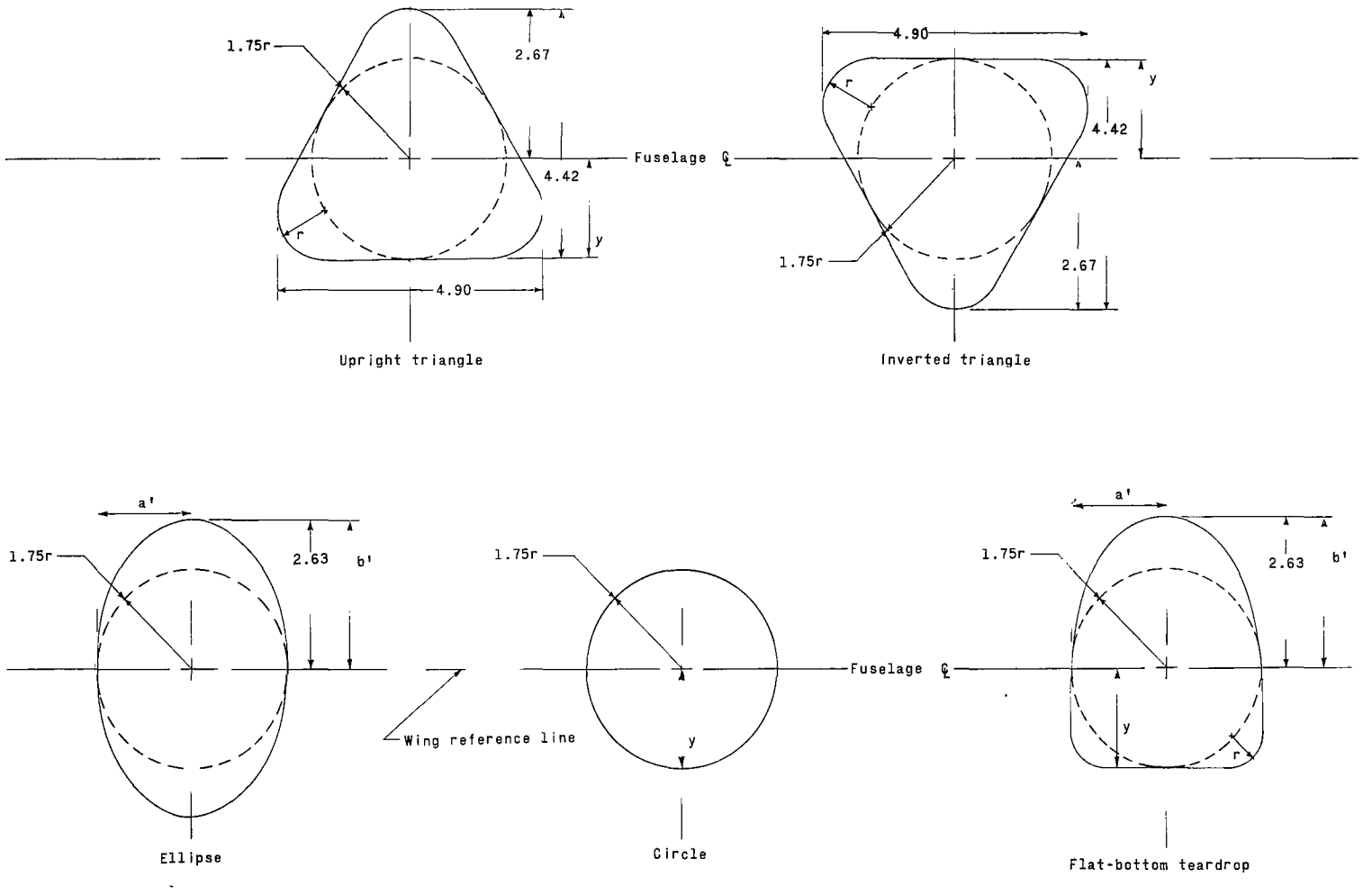

(b) Fuselage cross sections.

Figure 1.- Concluded.

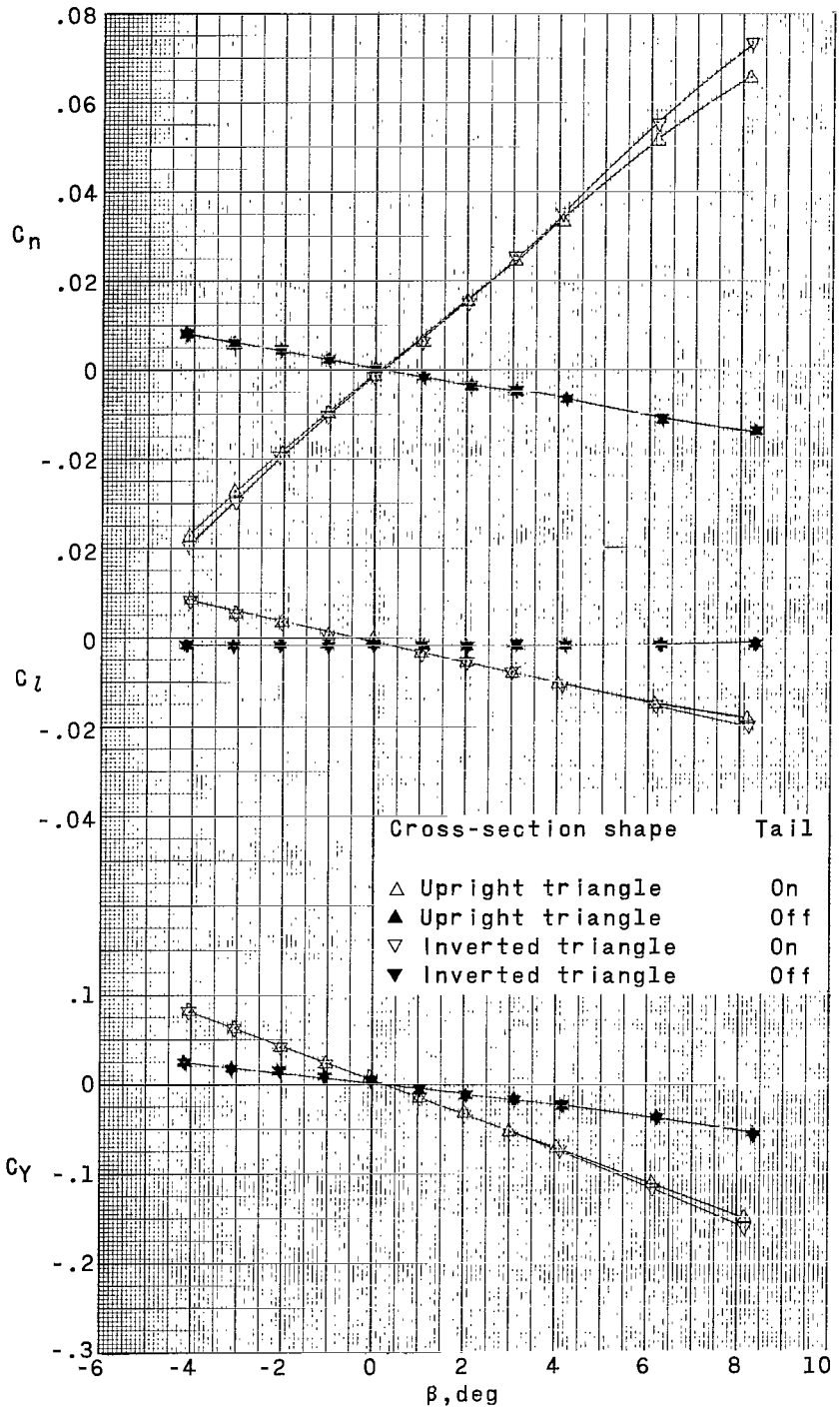

(a) Upright and inverted triangle; $\alpha \approx 0^{\circ}$.

Figure 2.- Typical aerodynamic characteristics in sideslip. Wing on; M = 1.41.

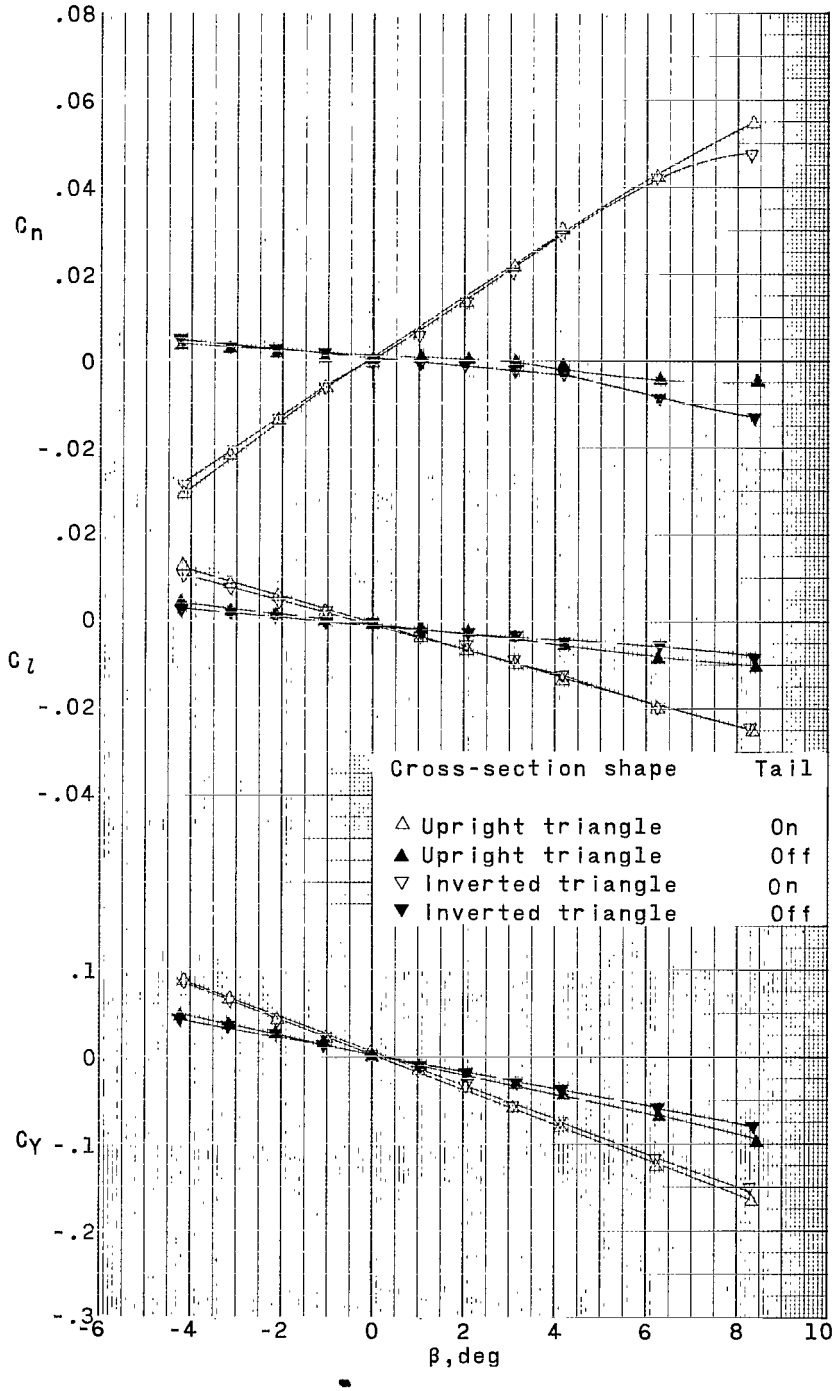

(a) Upright and inverted triangle; $\alpha \approx 11^{\circ}$ - Continued.

Figure 2.- Continued.

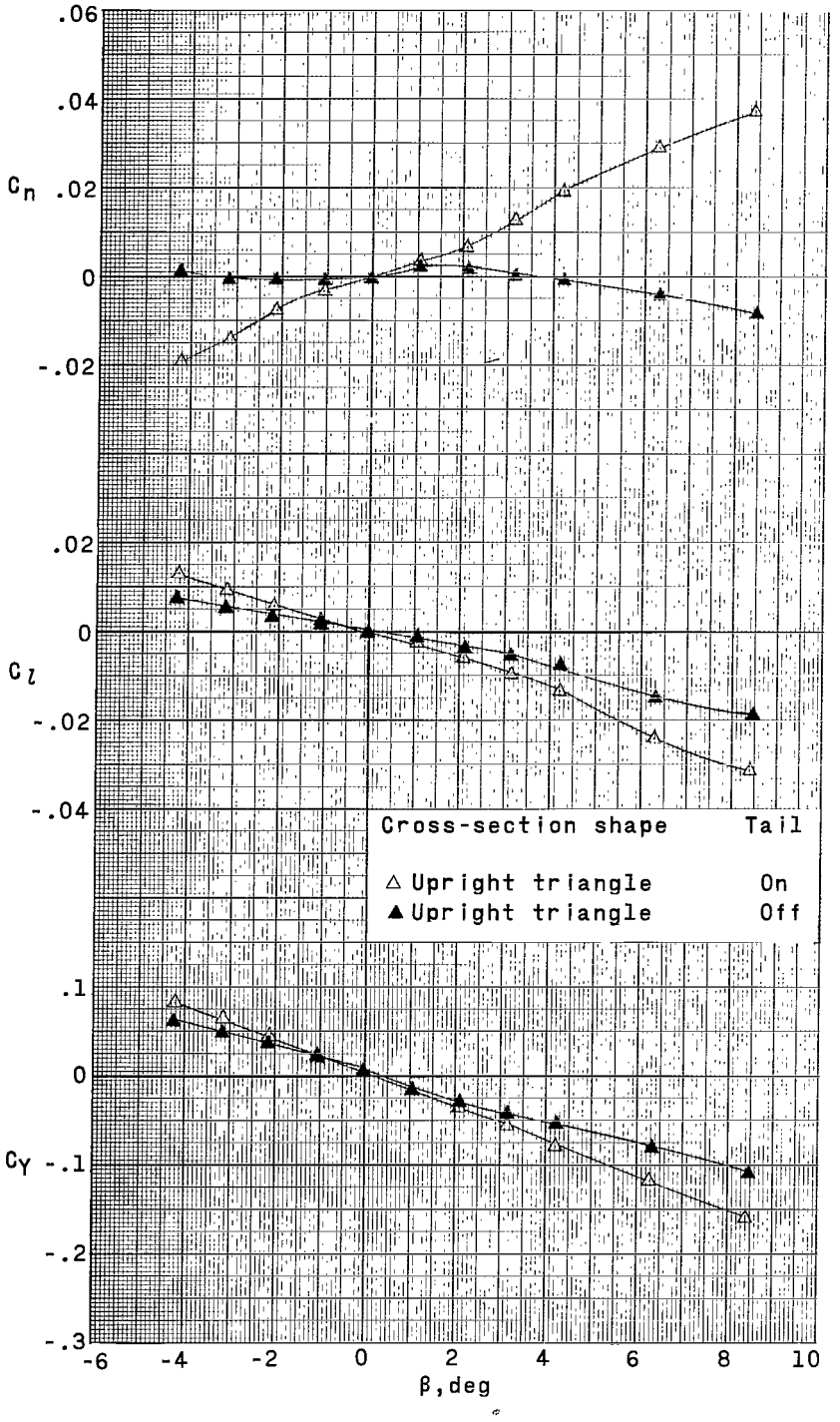

(a) Upright and inverted triangle; $\alpha \approx 16^{\circ}$ - Concluded.

Figure 2.- Continued.

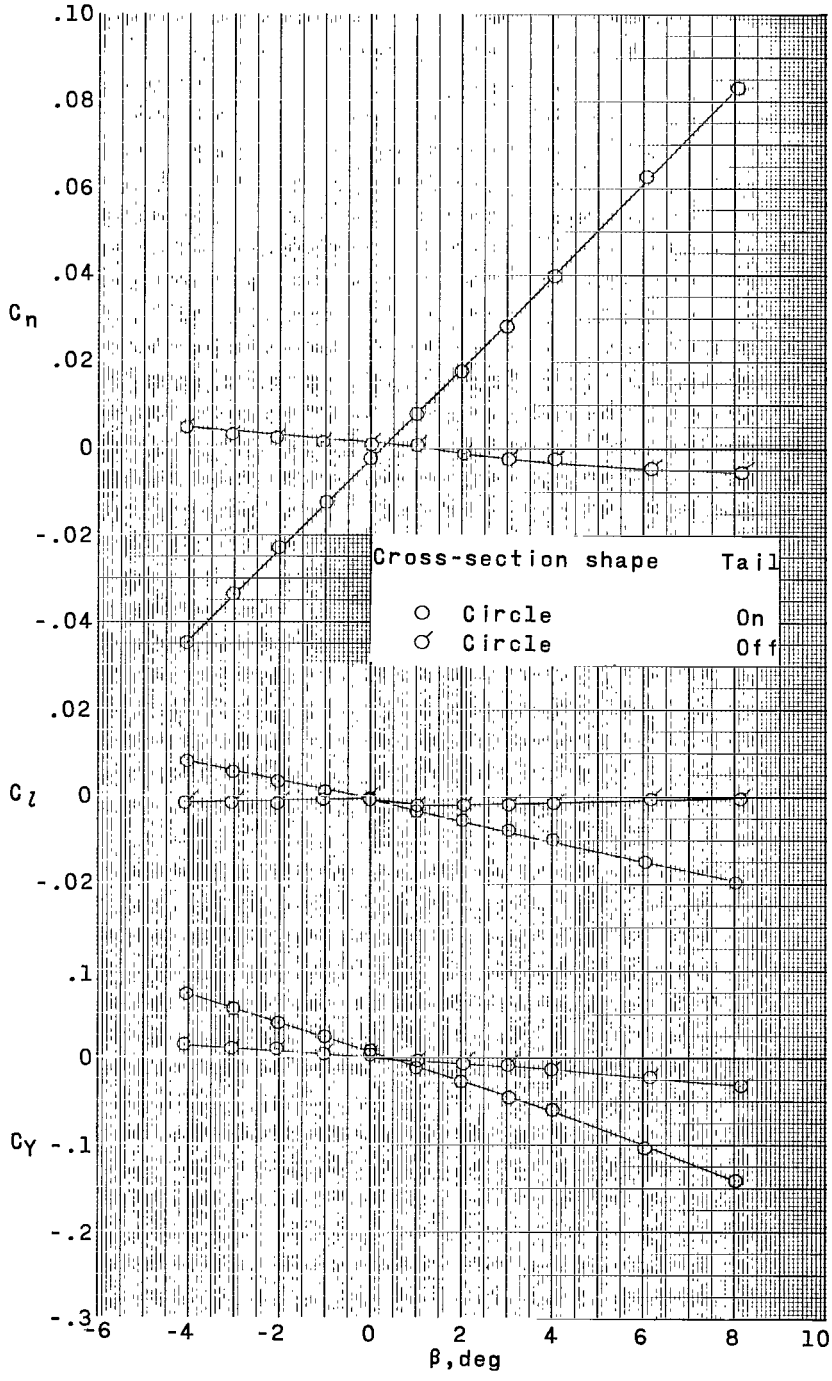

(b) Circle; $\alpha \approx 0^{\circ}$.

Figure 2.- Continued.

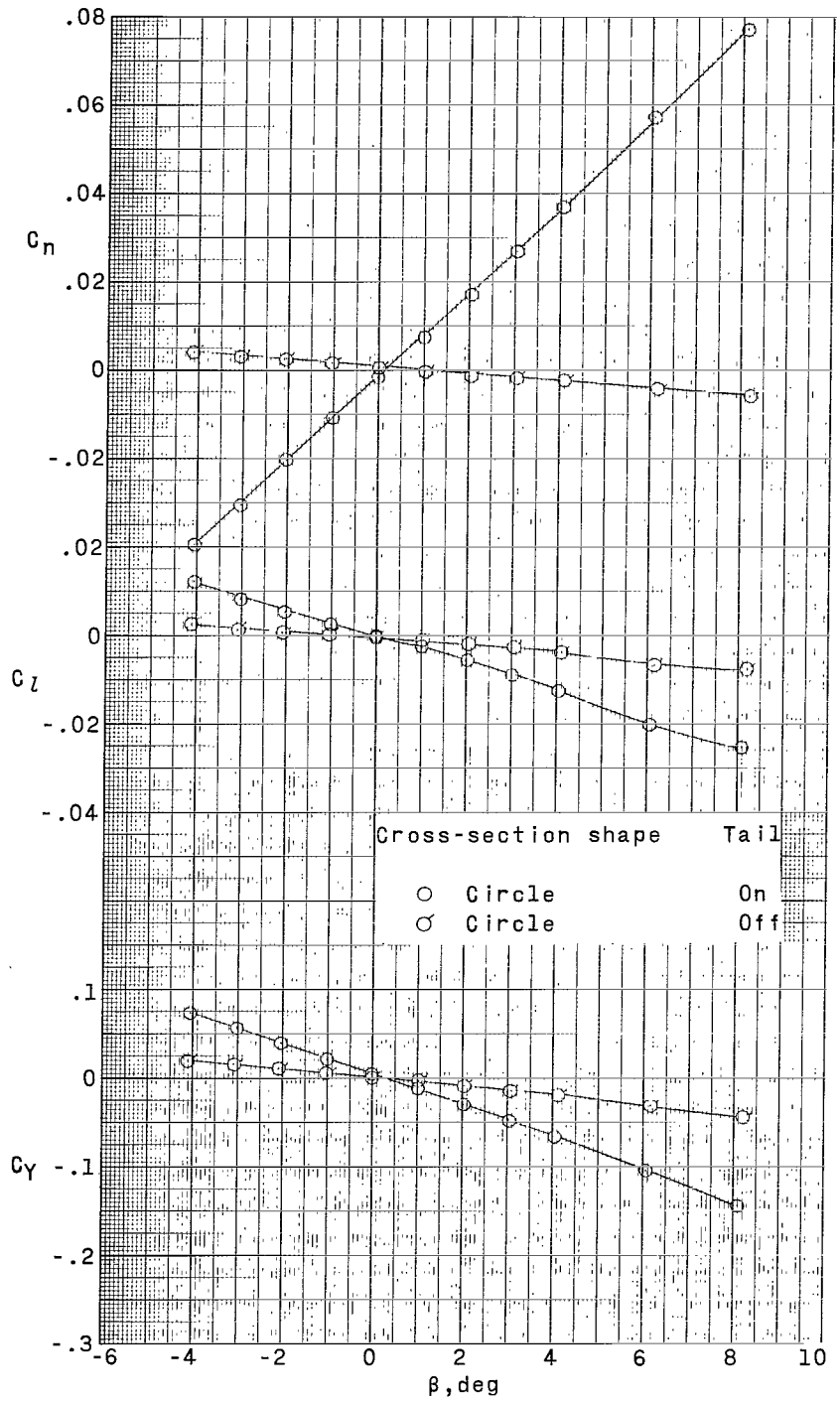

(b) Circle; $\alpha \approx 11^{\circ}$ - Continued.

Figure 2.- Continued.

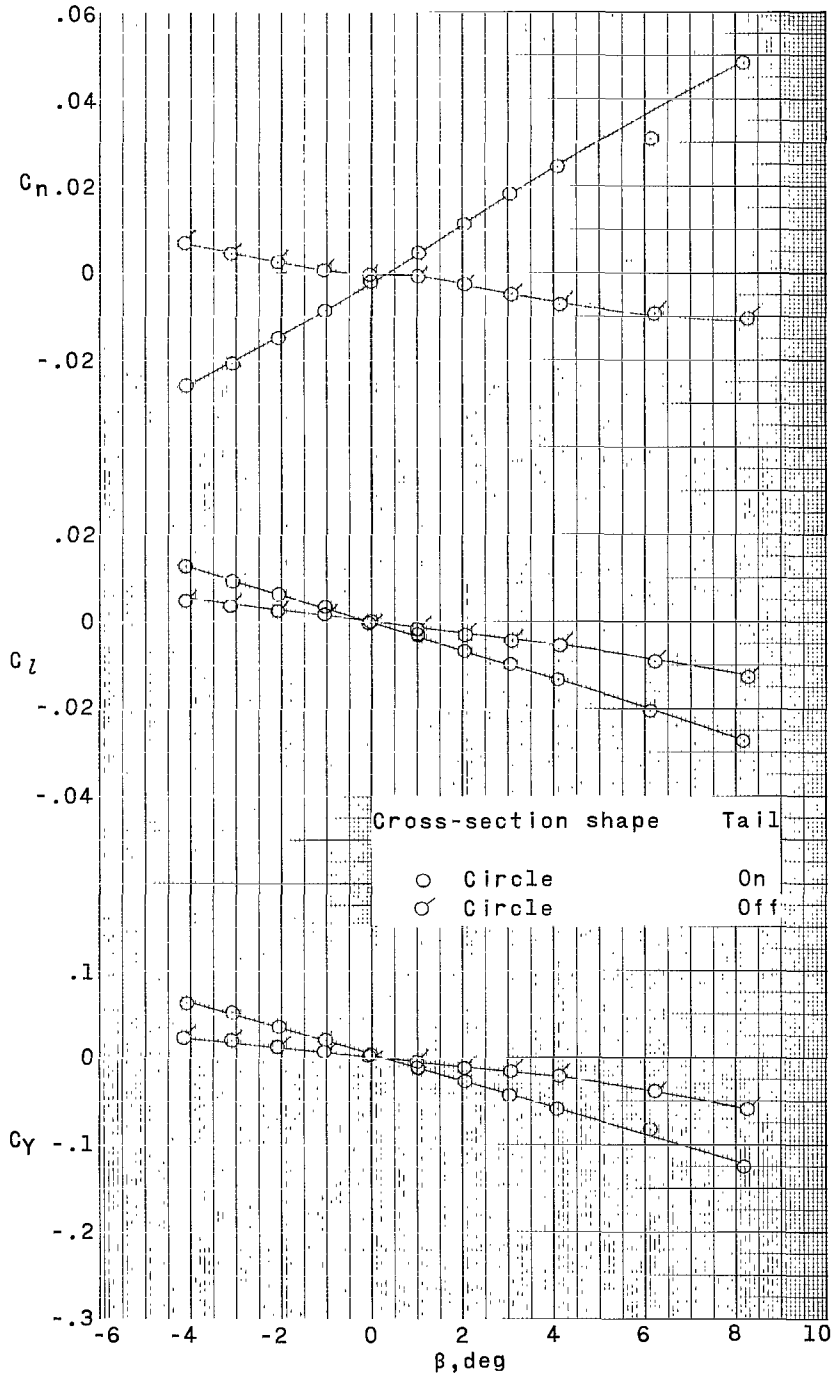

(b) Circle; $\alpha \approx 16^{\circ}$ - Concluded.

Figure 2.- Concluded.

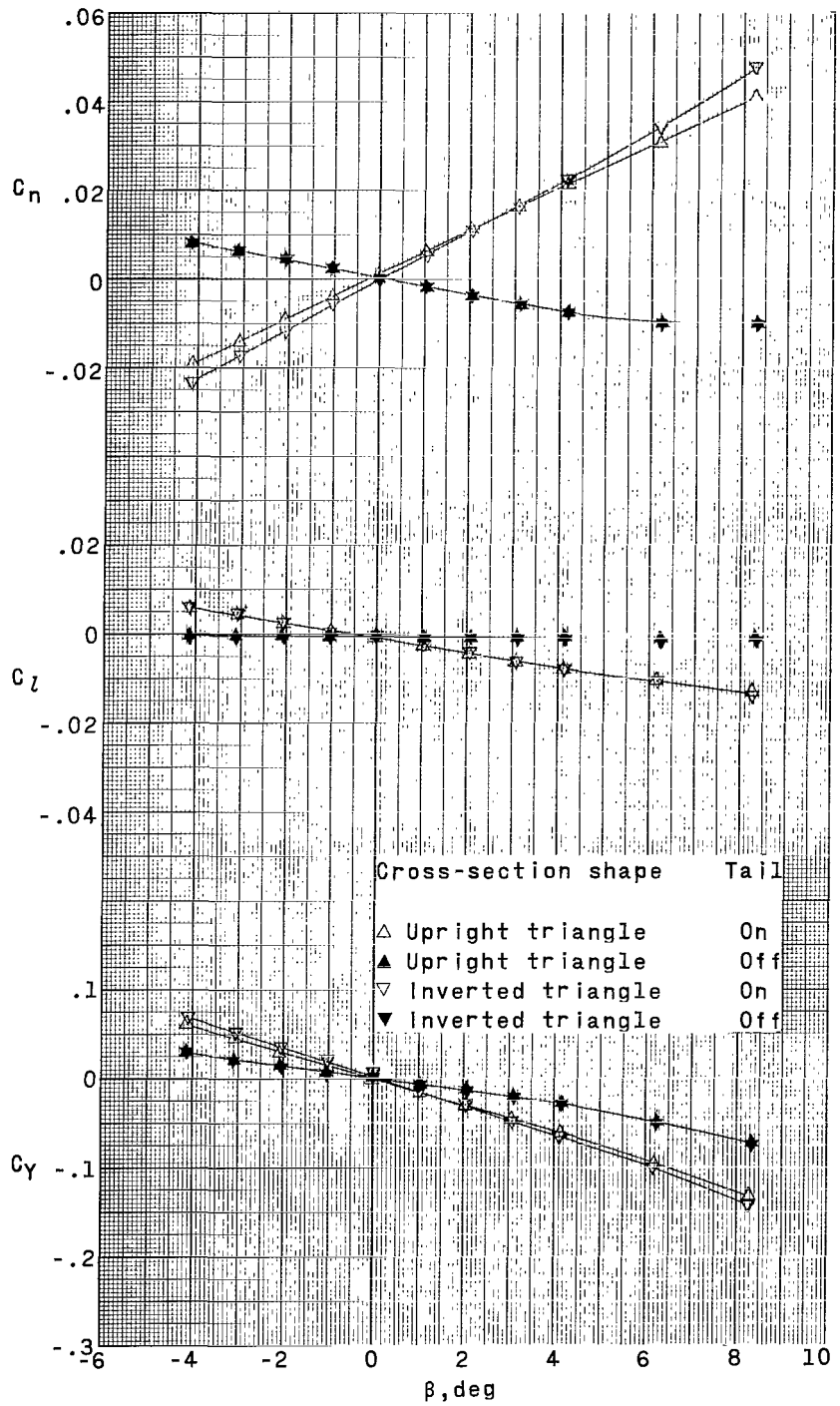

(a) Upright and inverted triangle; $\alpha \approx 0^{\circ}$.

Figure 3.- Typical aerodynamic characteristics in sideslip. Wing on; M = 2.20.

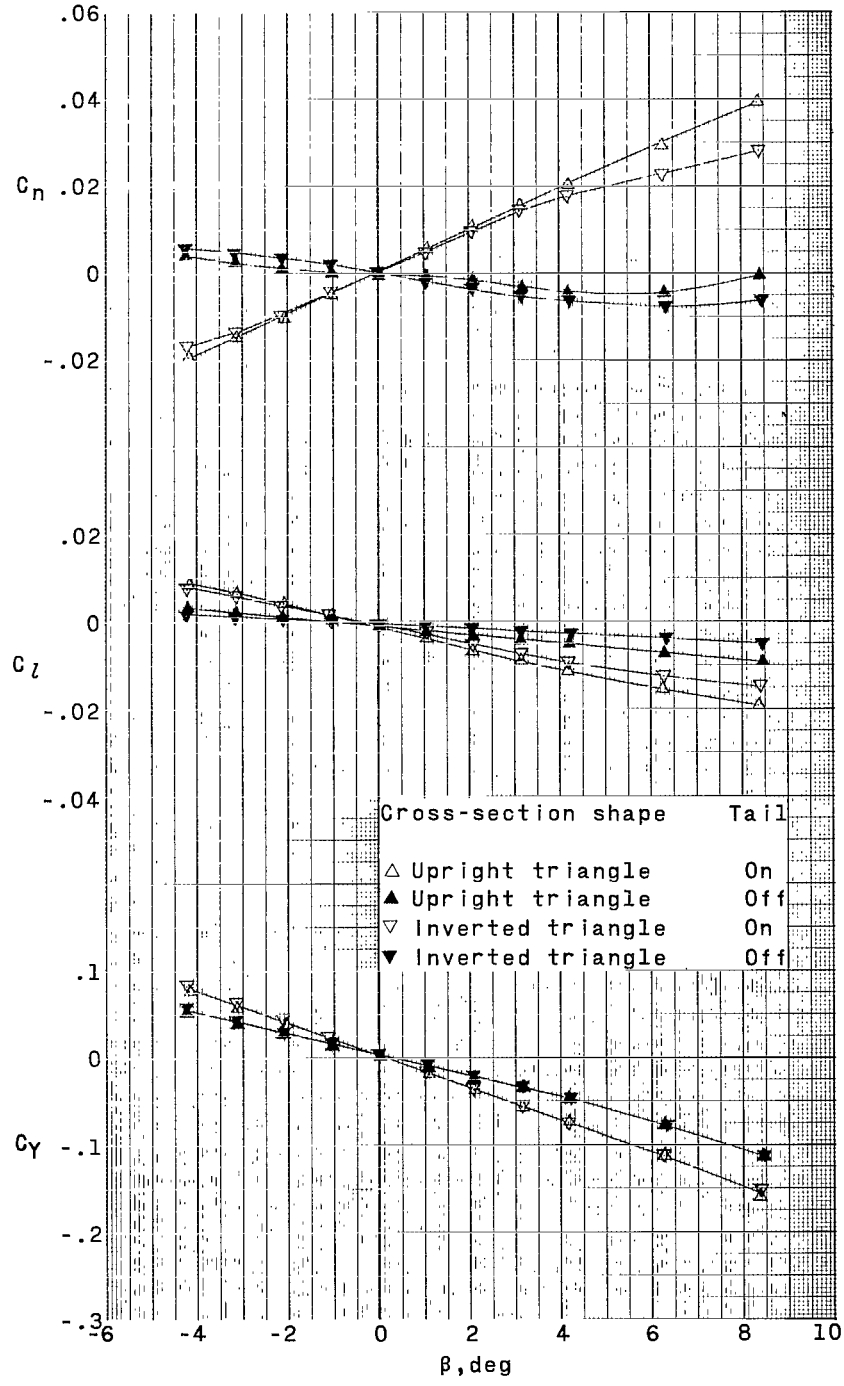

(a) Upright and inverted triangle; $\alpha \approx 11^{\circ}$ - Continued.

Figure 3.- Continued.

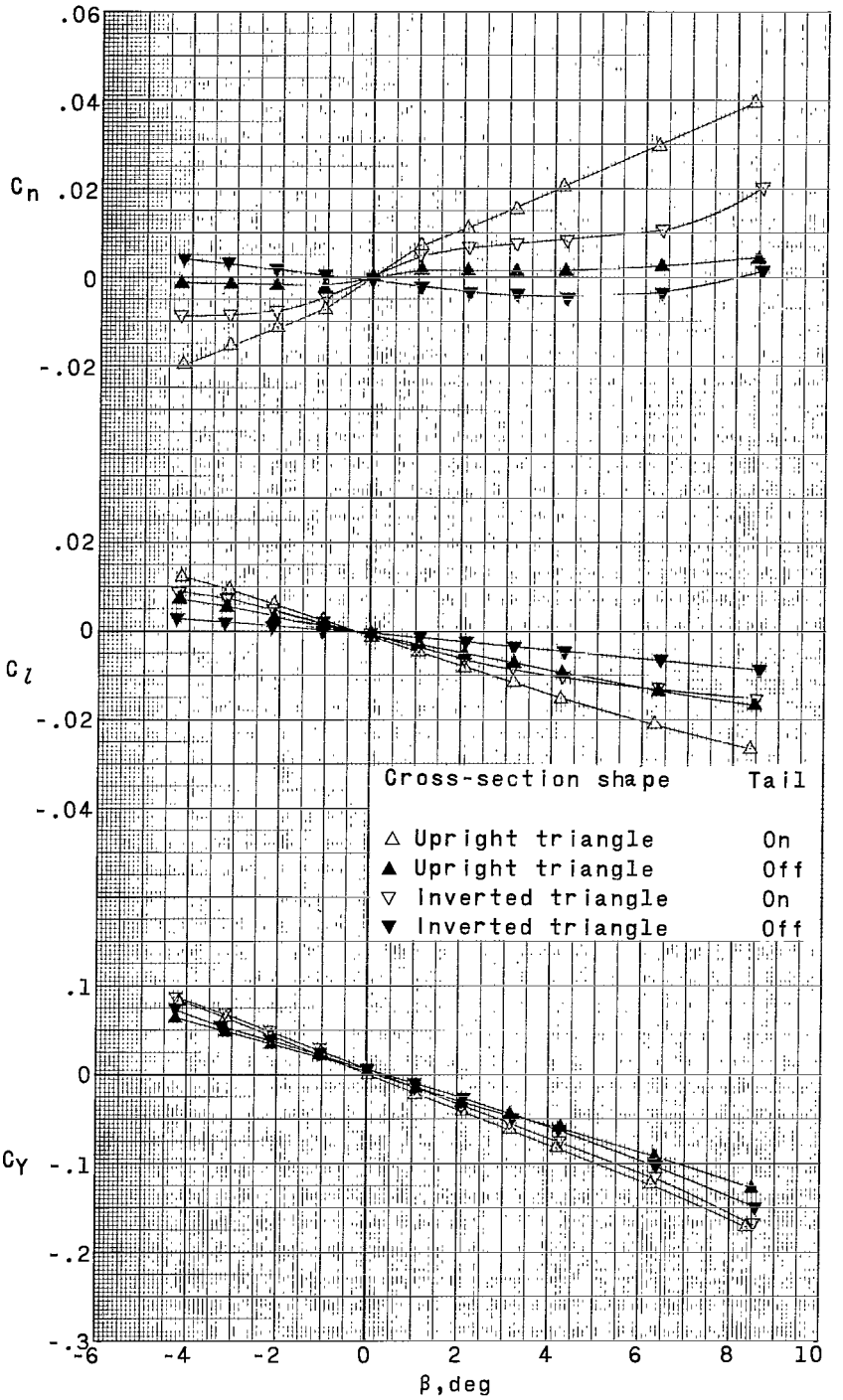

(a) Upright and inverted triangle; $\alpha \approx 16^{\circ}$ - Concluded.

Figure 3.- Continued.

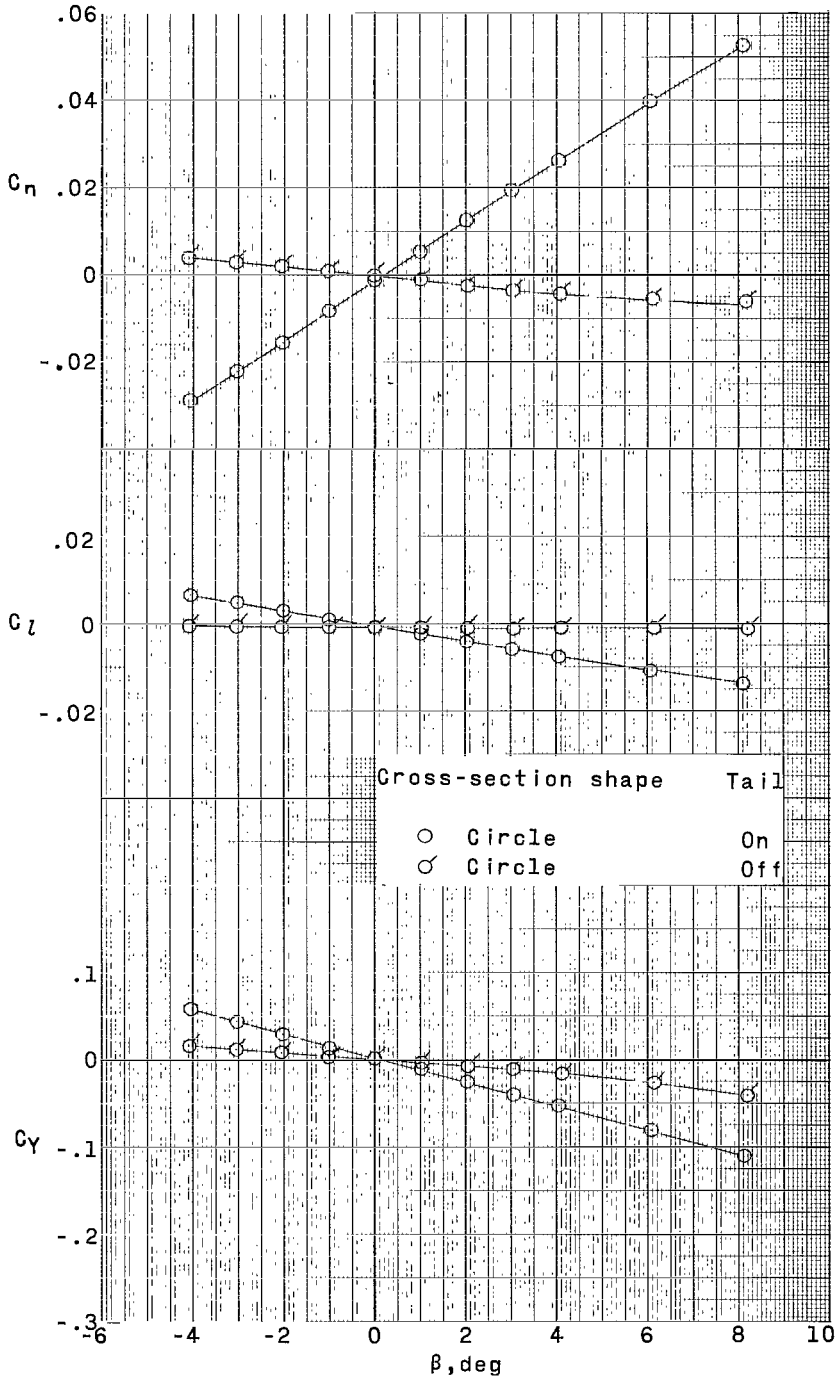

(b) Circle; $\alpha \approx 0^{o}$.

Figure 3.- Continued.

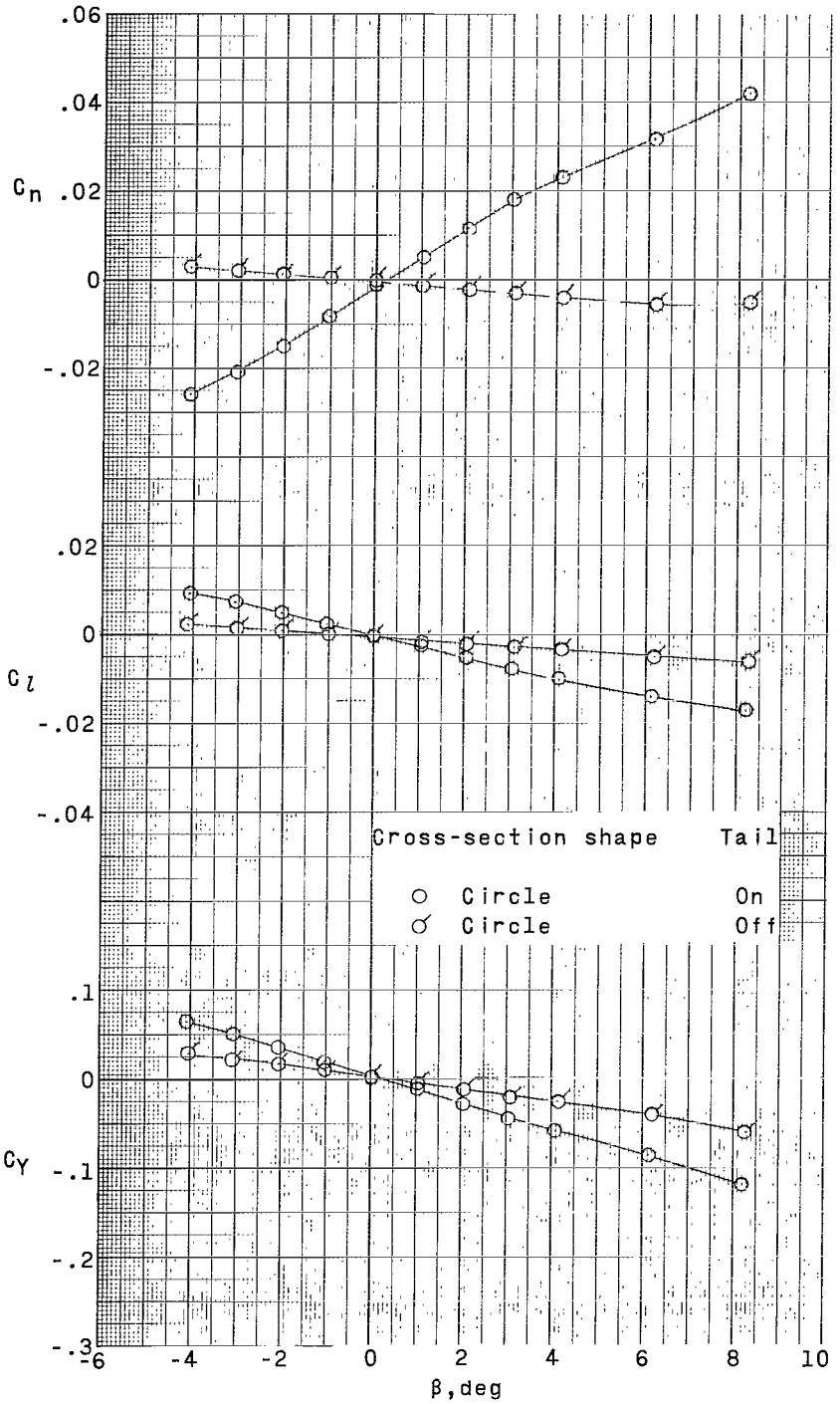

(b) Circle; $\alpha \approx 11^{\circ}$ - Continued.

Figure 3.- Continued.

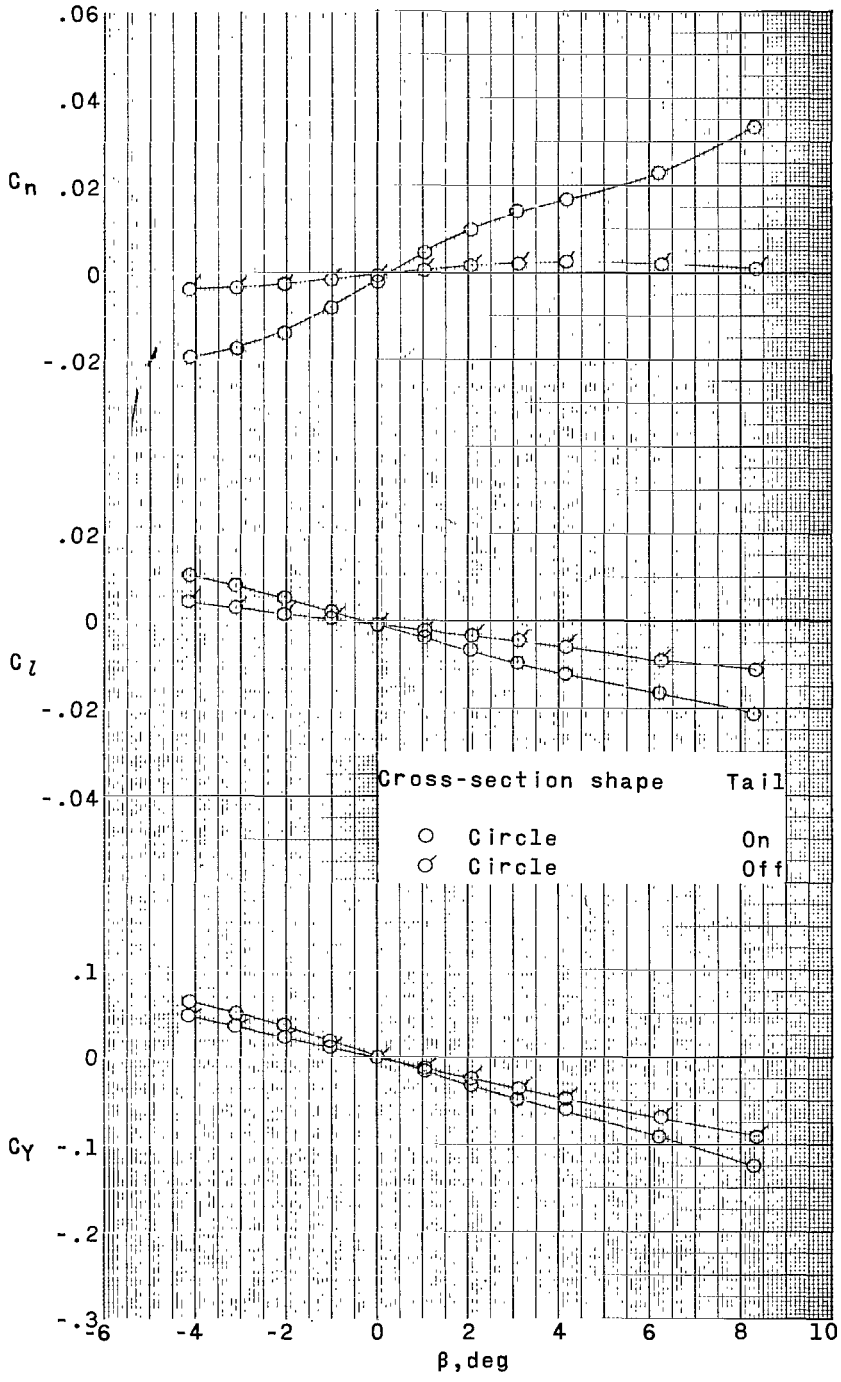

(b) Circle; $\alpha \approx 16^{\circ}$ - Concluded.

Figure 3.- Concluded.

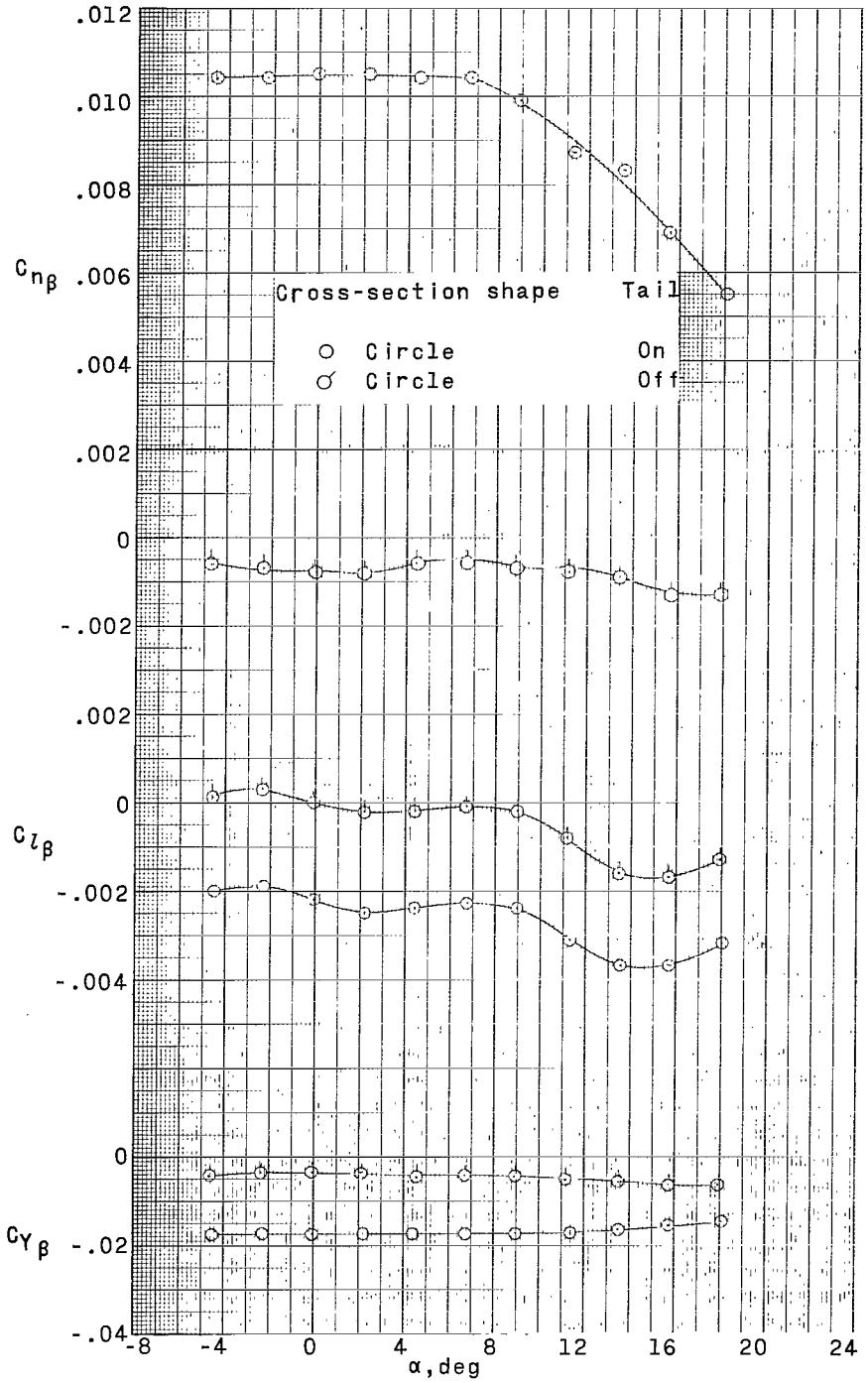

(a) M = 1.41.

Figure 4.- Variation of sideslip parameters with angle of attack for the circular fuselage. Wing on.

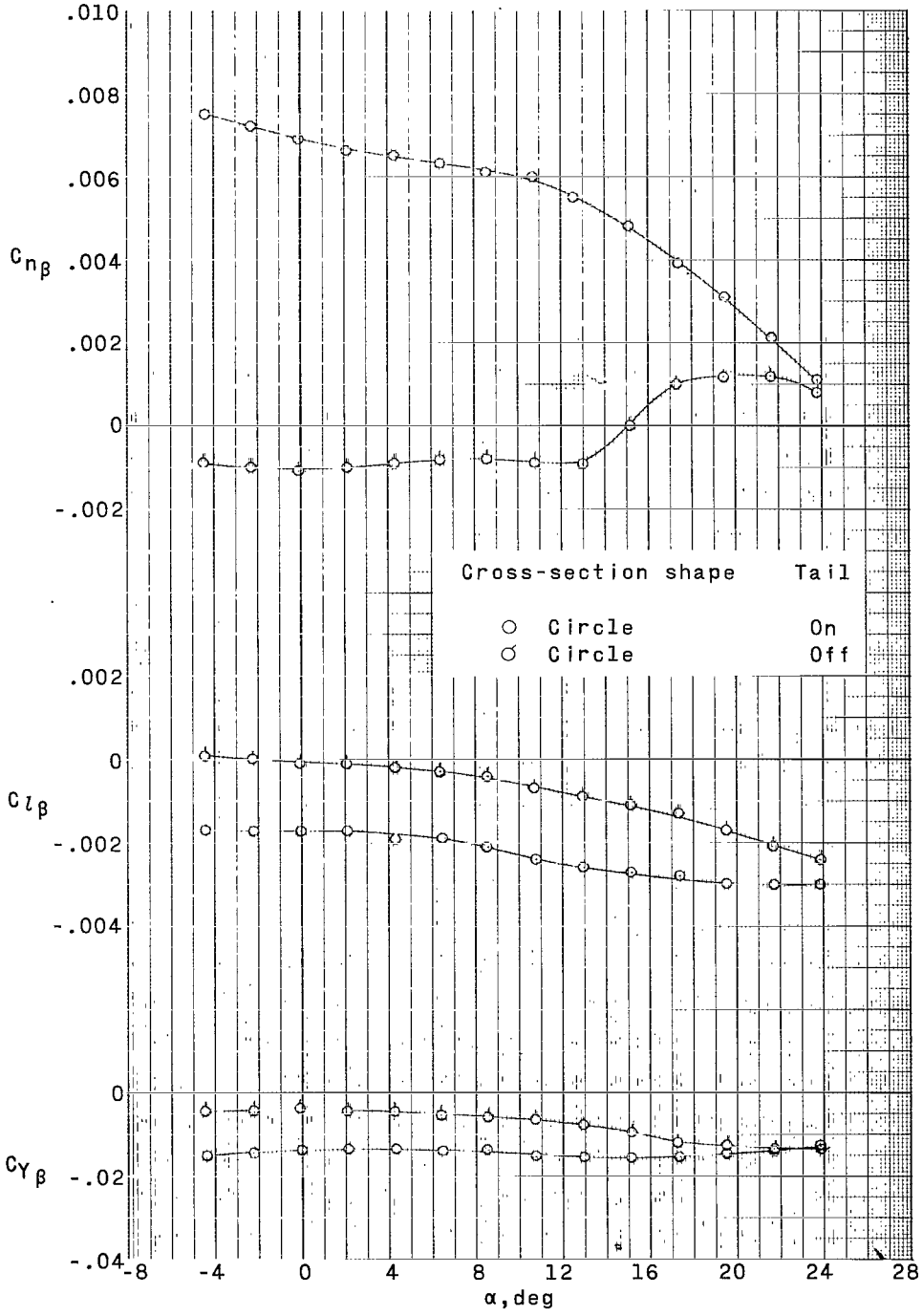

(b) M = 2.20.

Figure 4.- Concluded.

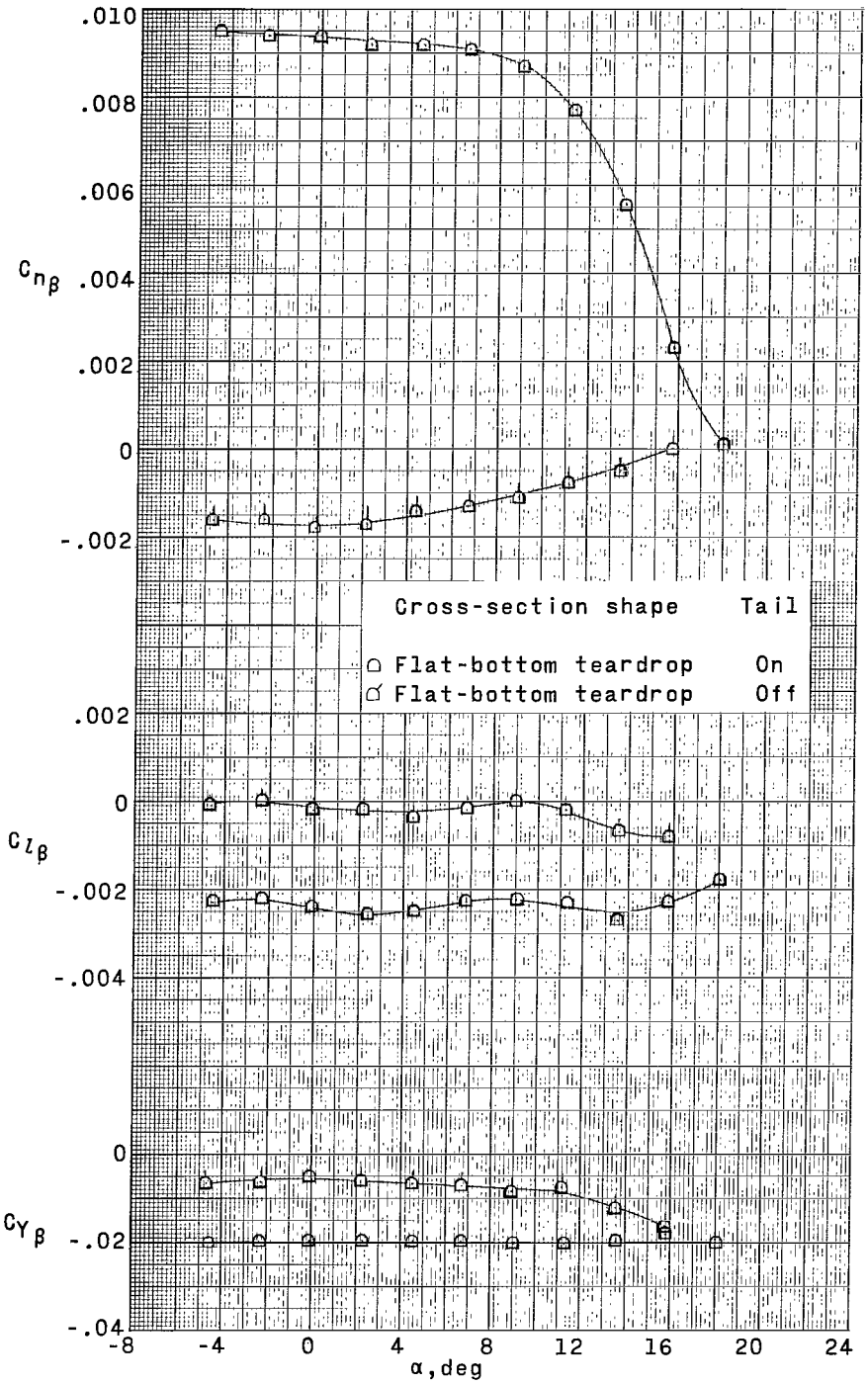

(a) M = 1.41.

Figure 5.- Variation of sideslip parameters with angle of attack for the flat-bottom teardrop fuselage. Wing on.

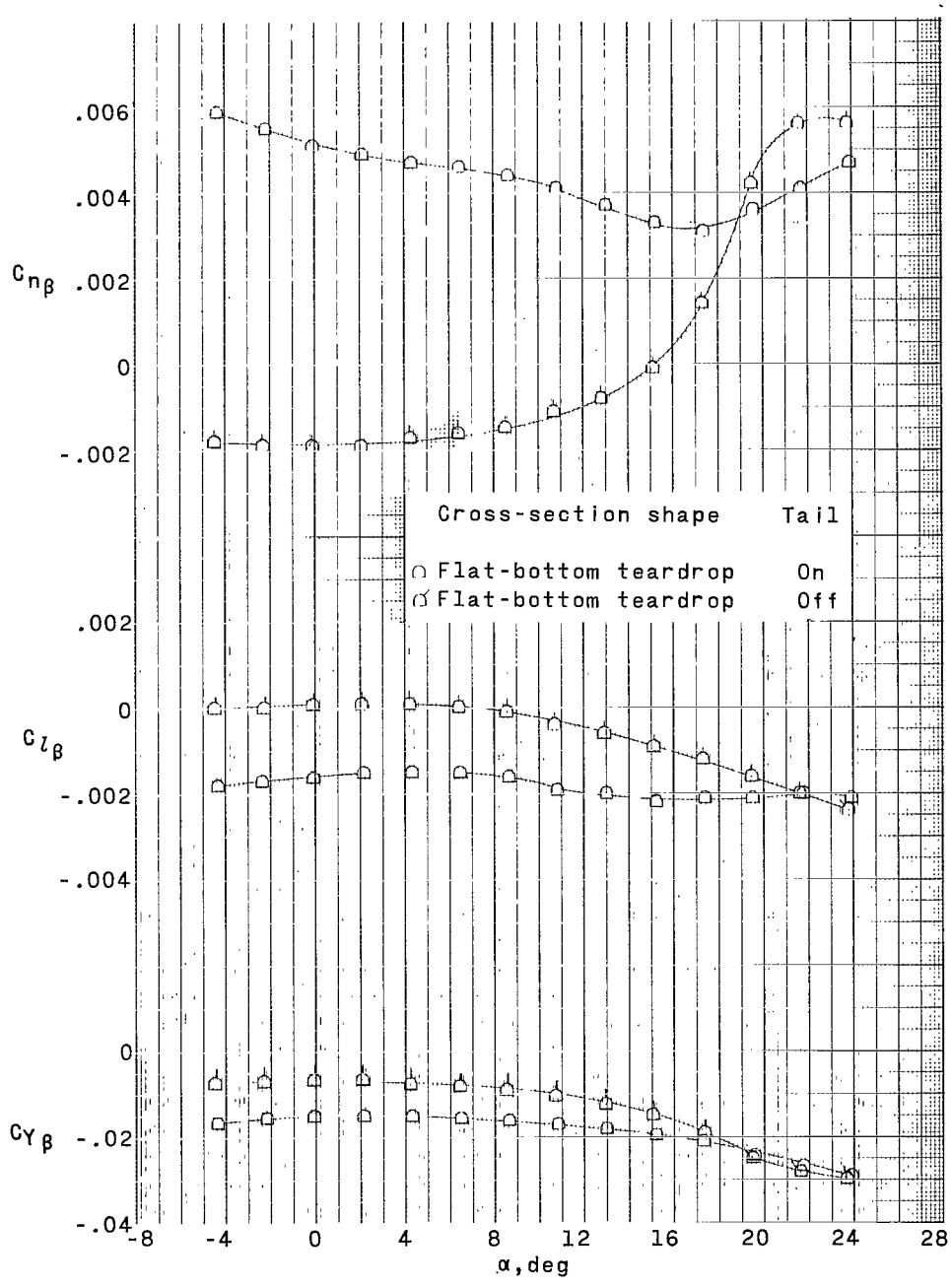

(b) M = 2.20.

Figure 5.- Concluded.

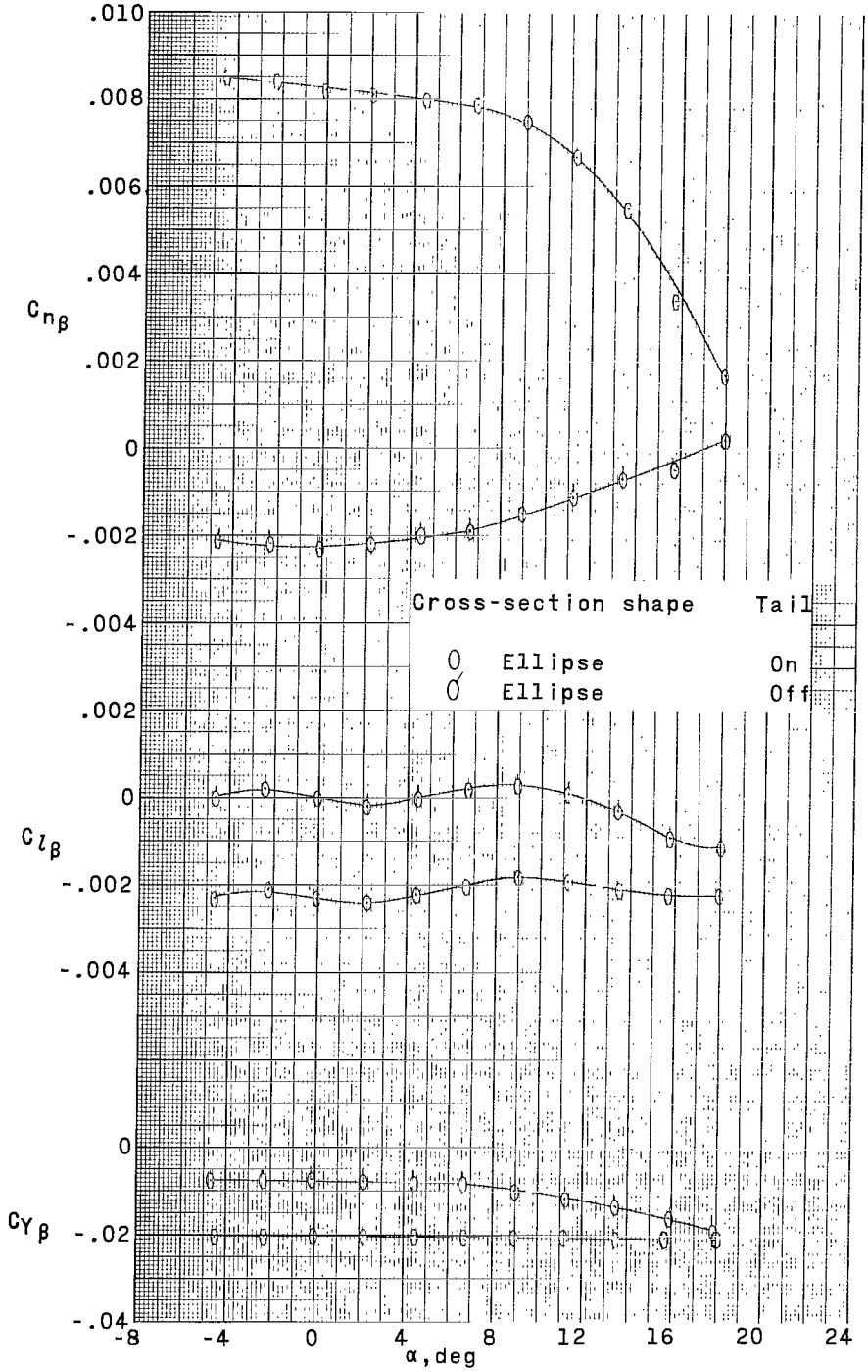

(a) M = 1.41.

Figure 6.- Variation of sideslip parameters with angle of attack for an elliptical fuselage. Wing on.

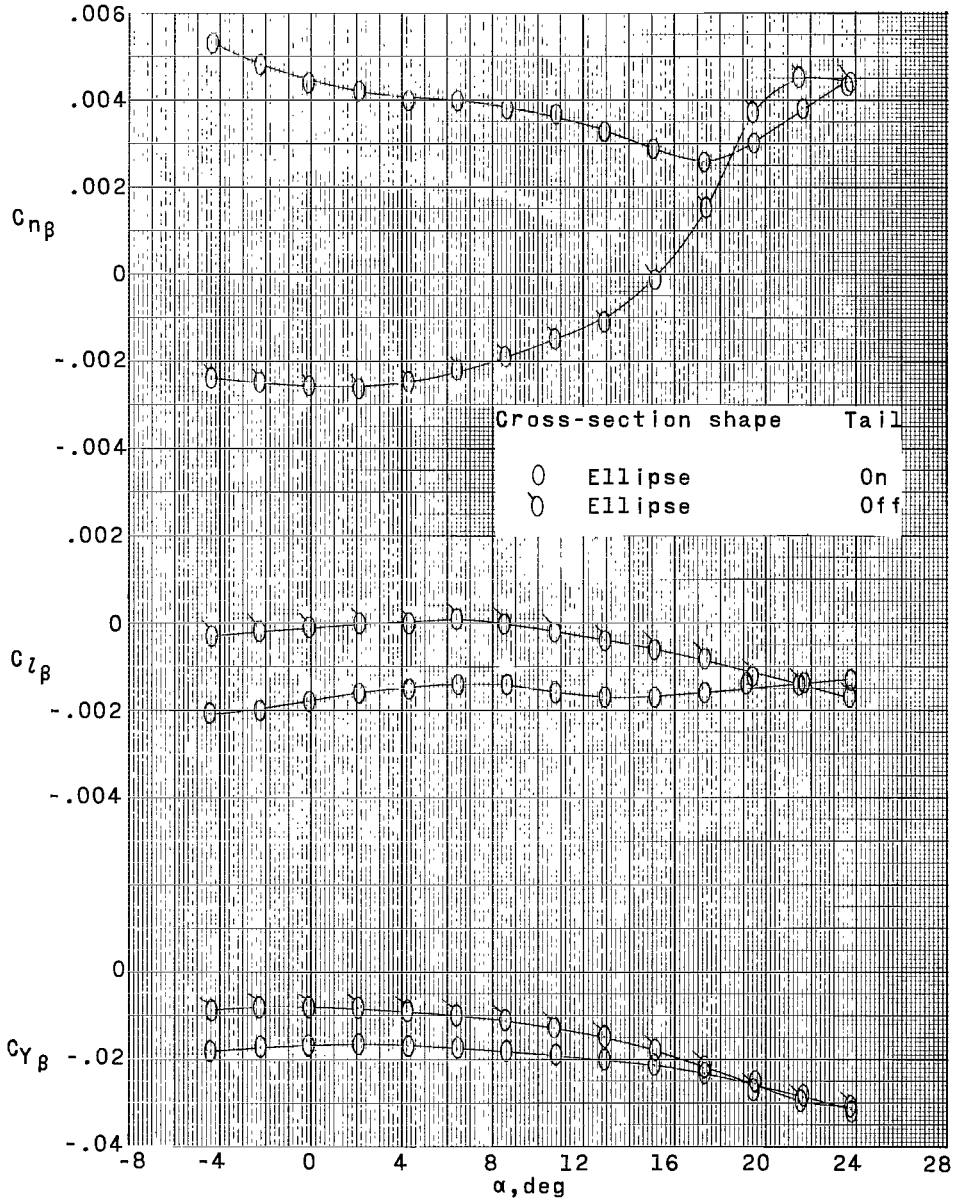

(b) M = 2.20.

Figure 6.- Concluded.

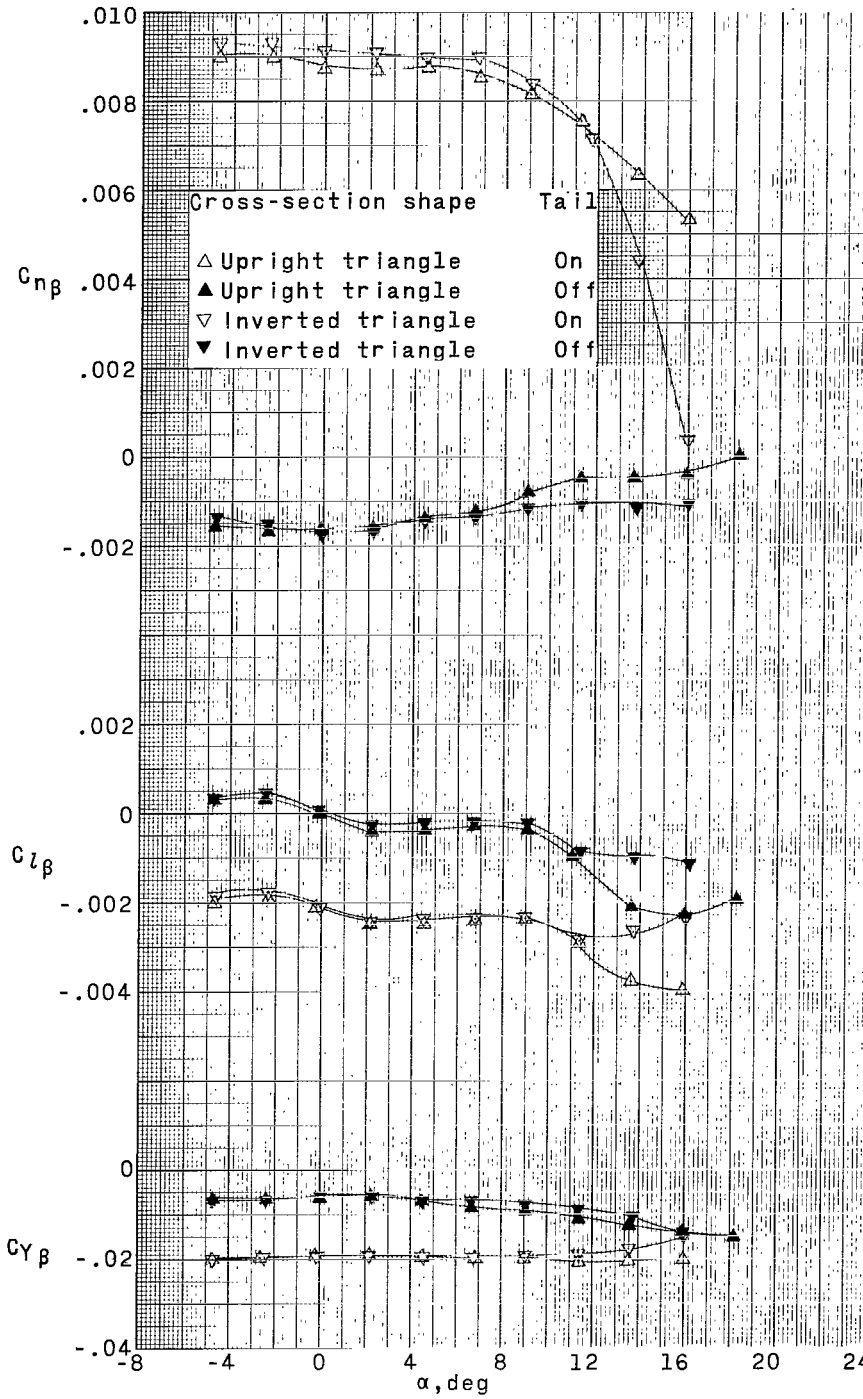

(a) M = 1.41.

Figure 7.- Variation of sideslip parameters with angle of attack for the upright and inverted triangular fuselage. Wing on.

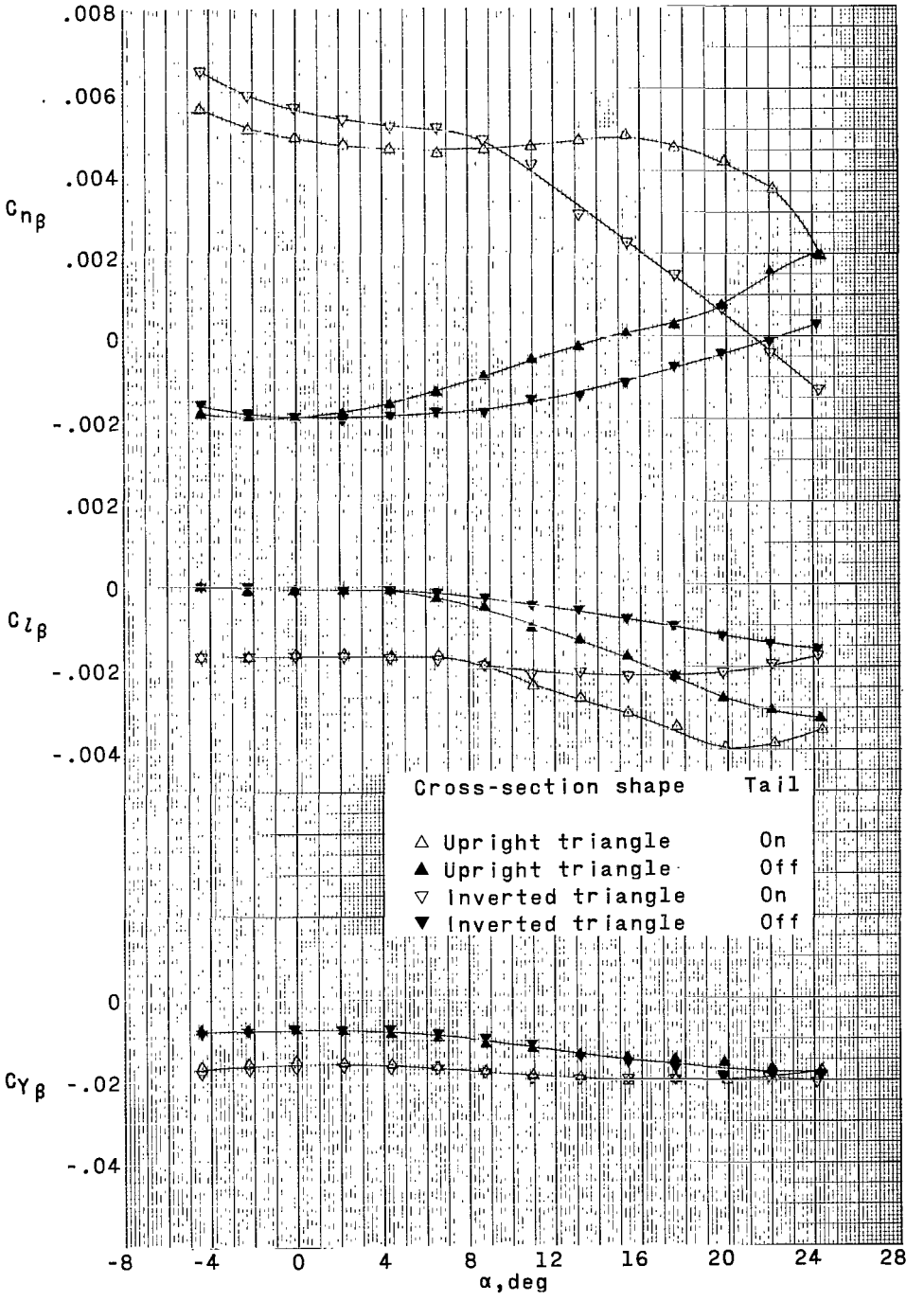

(b) M = 2.20.

Figure 7.- Concluded.

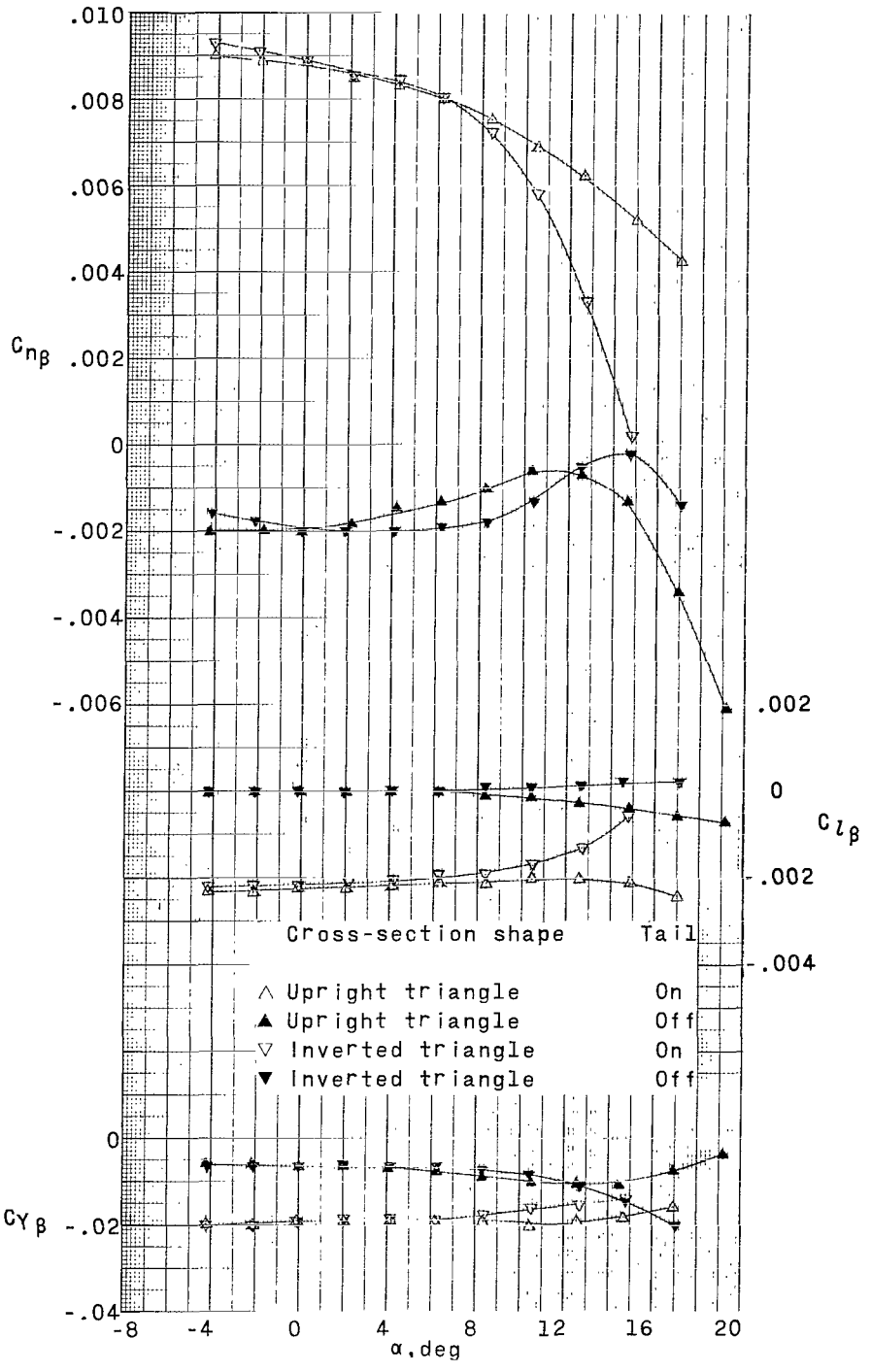

(a) M = 1.41.

Figure 8.- Variation of sideslip parameters with angle of attack for the upright and inverted triangular fuselage. Wing off.

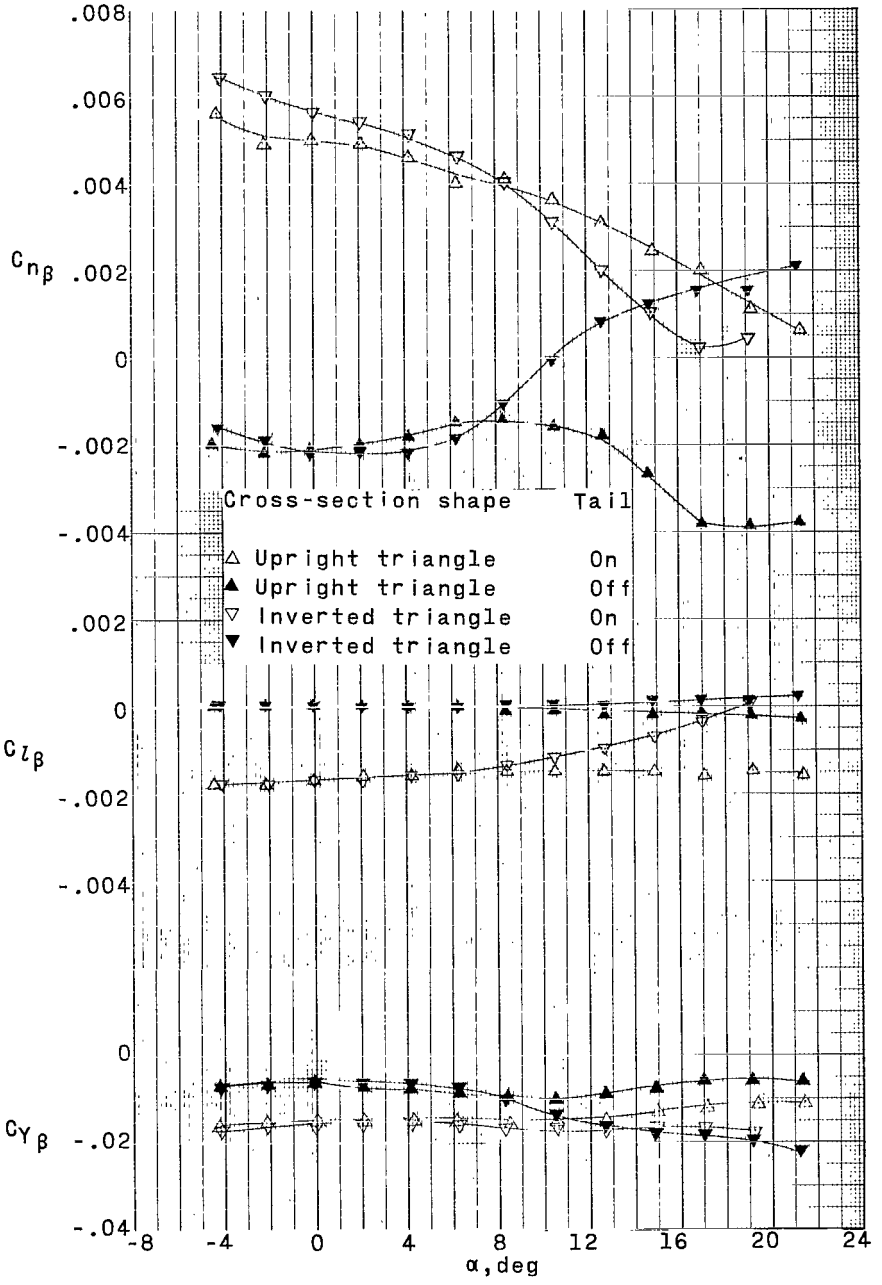

(b) M = 2.20.

Figure 8.- Concluded.

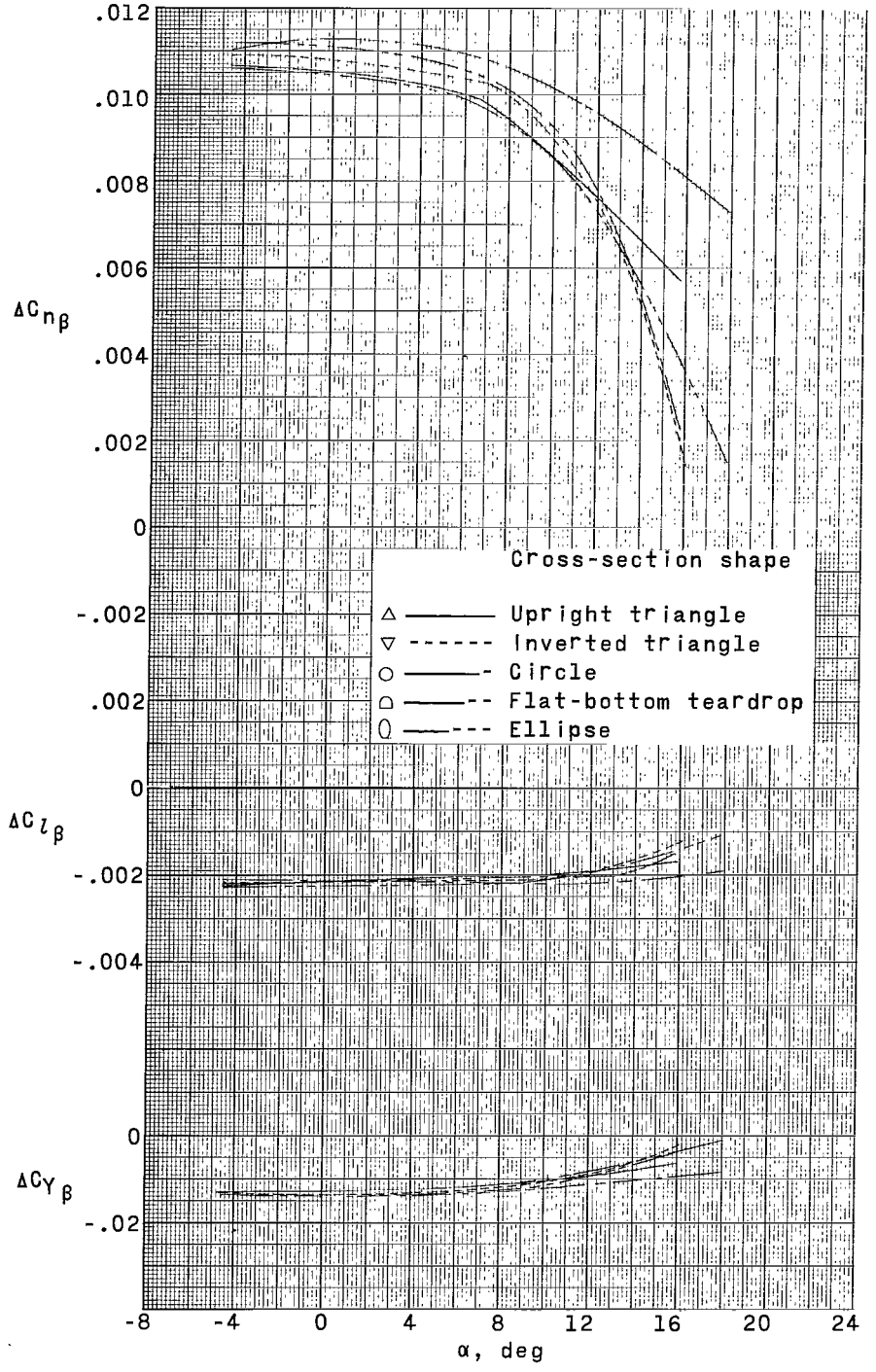

(a) M = 1.41.

Figure 9.- Variation of vertical-tail contribution to sideslip derivatives for various body shapes. Wing on.

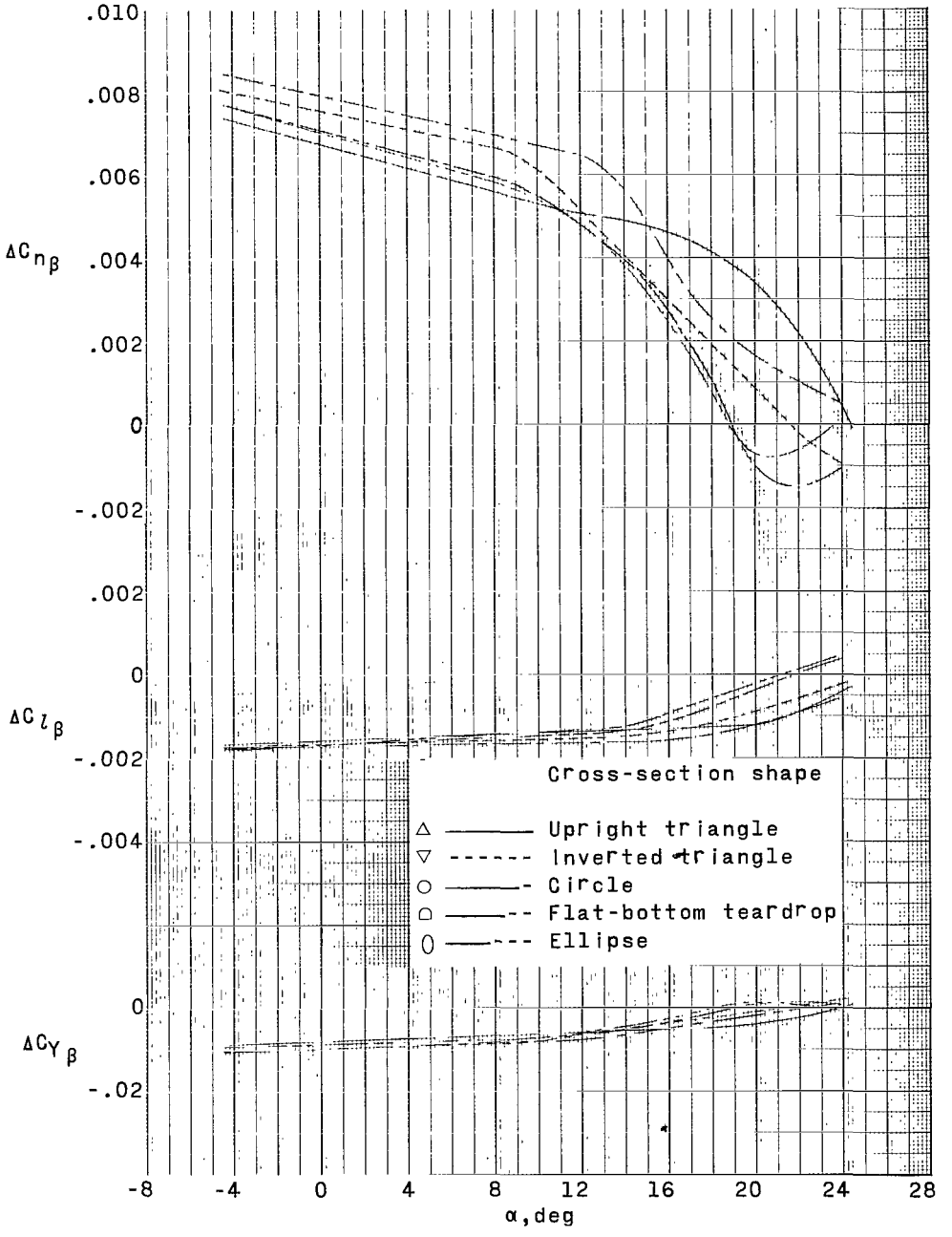

(b) M = 2.20.

Figure 9.- Concluded.

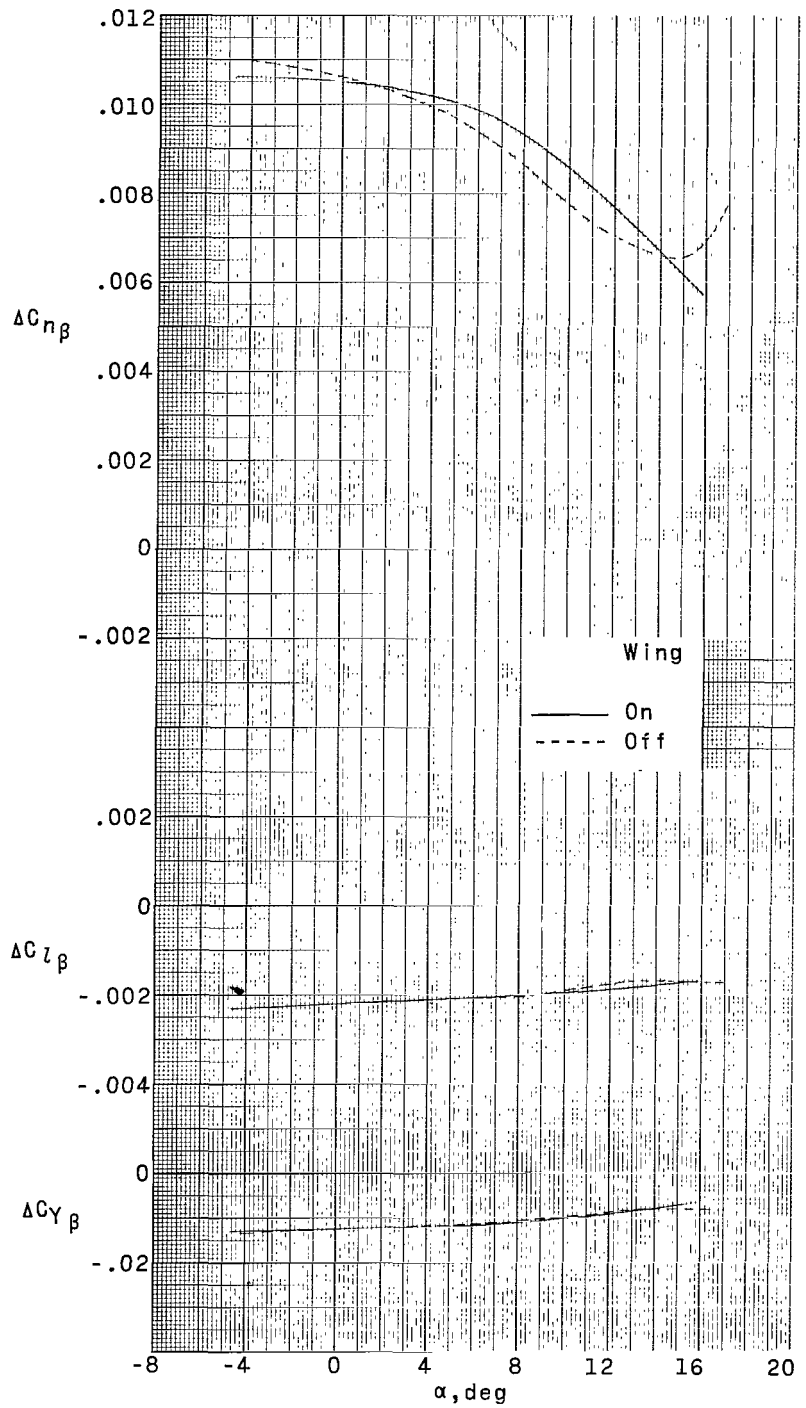

(a) M = 1.41; upright triangle.

Figure 10.- Effect of wing on the variation of vertical-tail contribution to sideslip derivatives for upright and inverted triangular bodies.

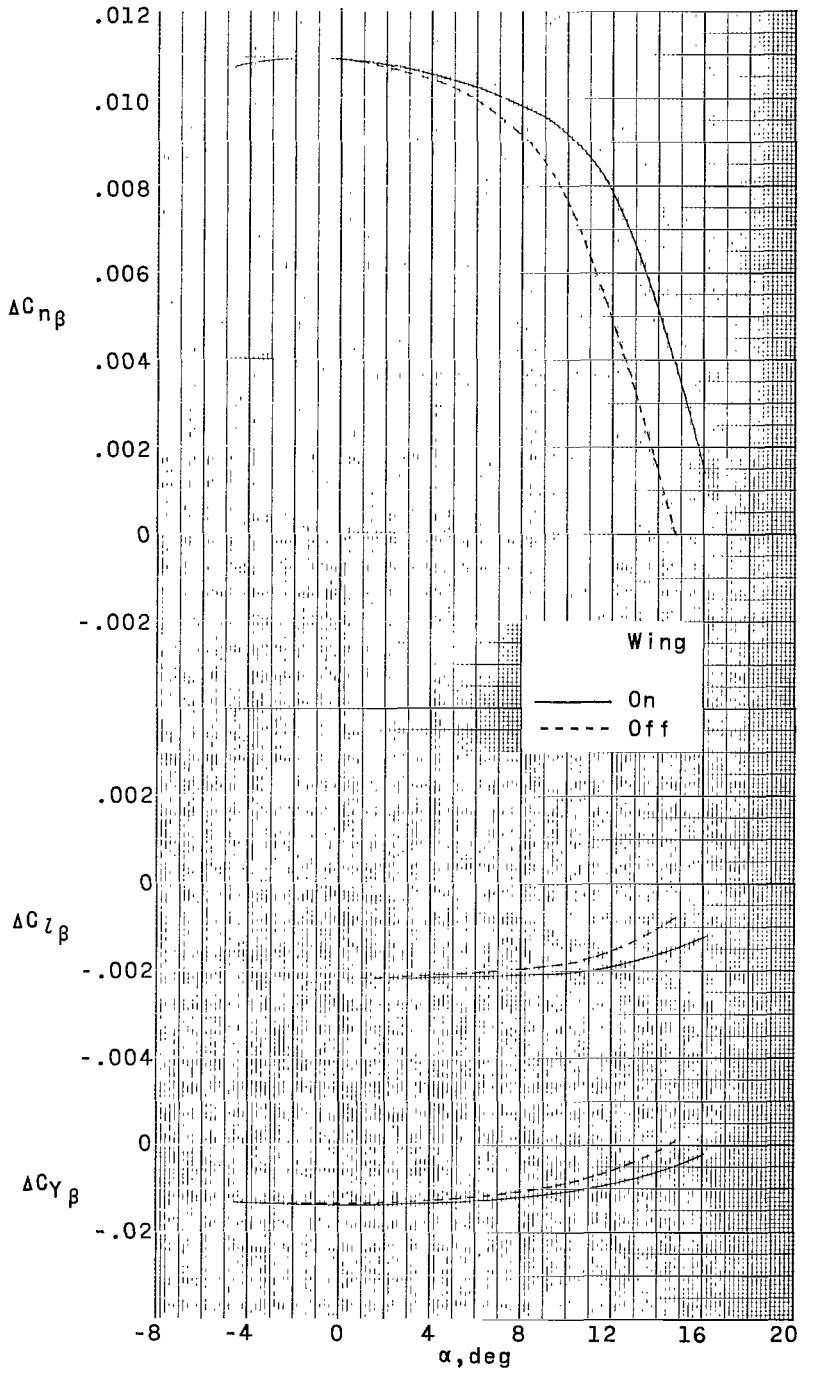

(b) M = 1.41; inverted triangle.

Figure 10.- Continued.

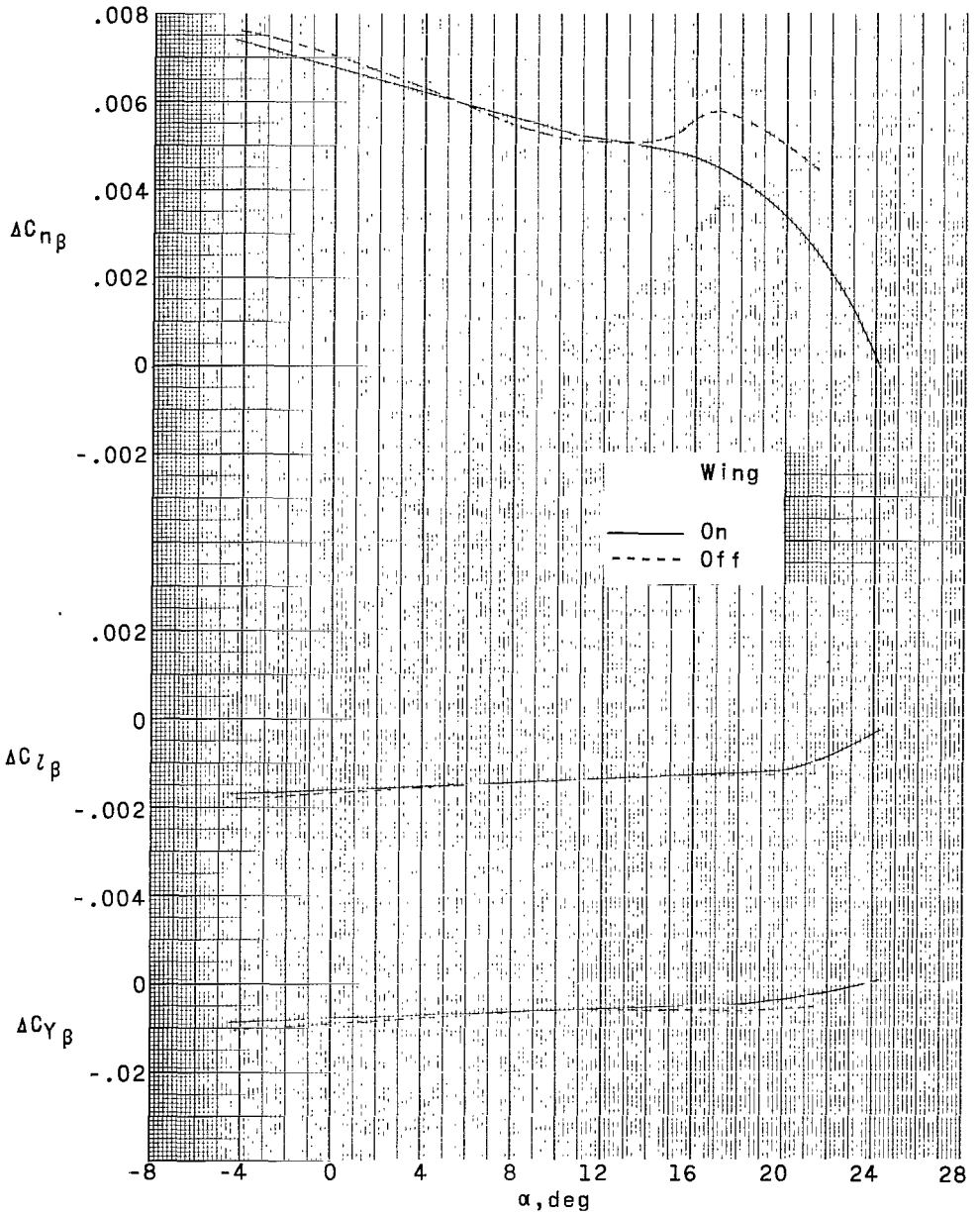

(c) M = 2.20; upright triangle.

Figure 10.- Continued.

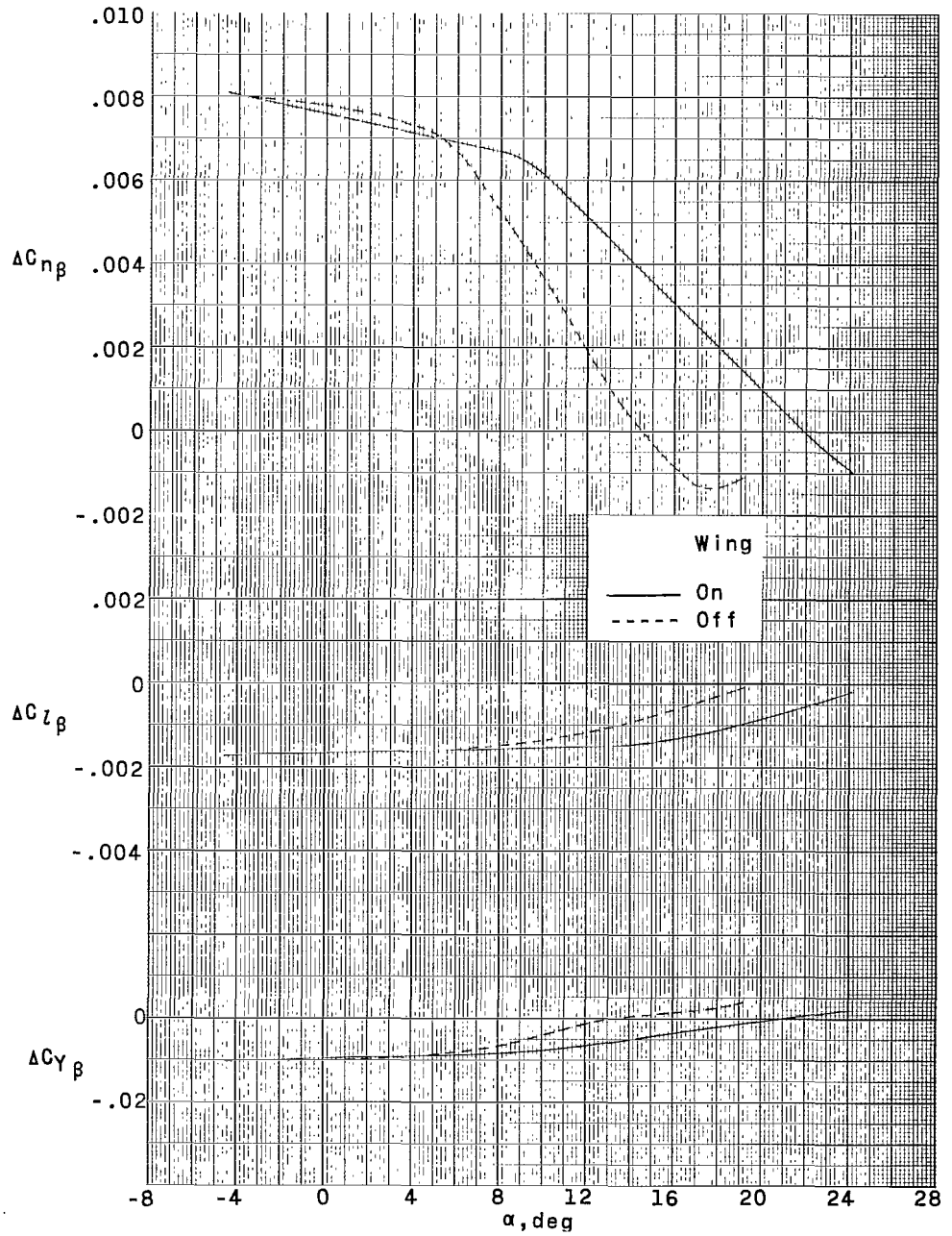

(d) M = 2.20; inverted triangle.

Figure 10.- Concluded.

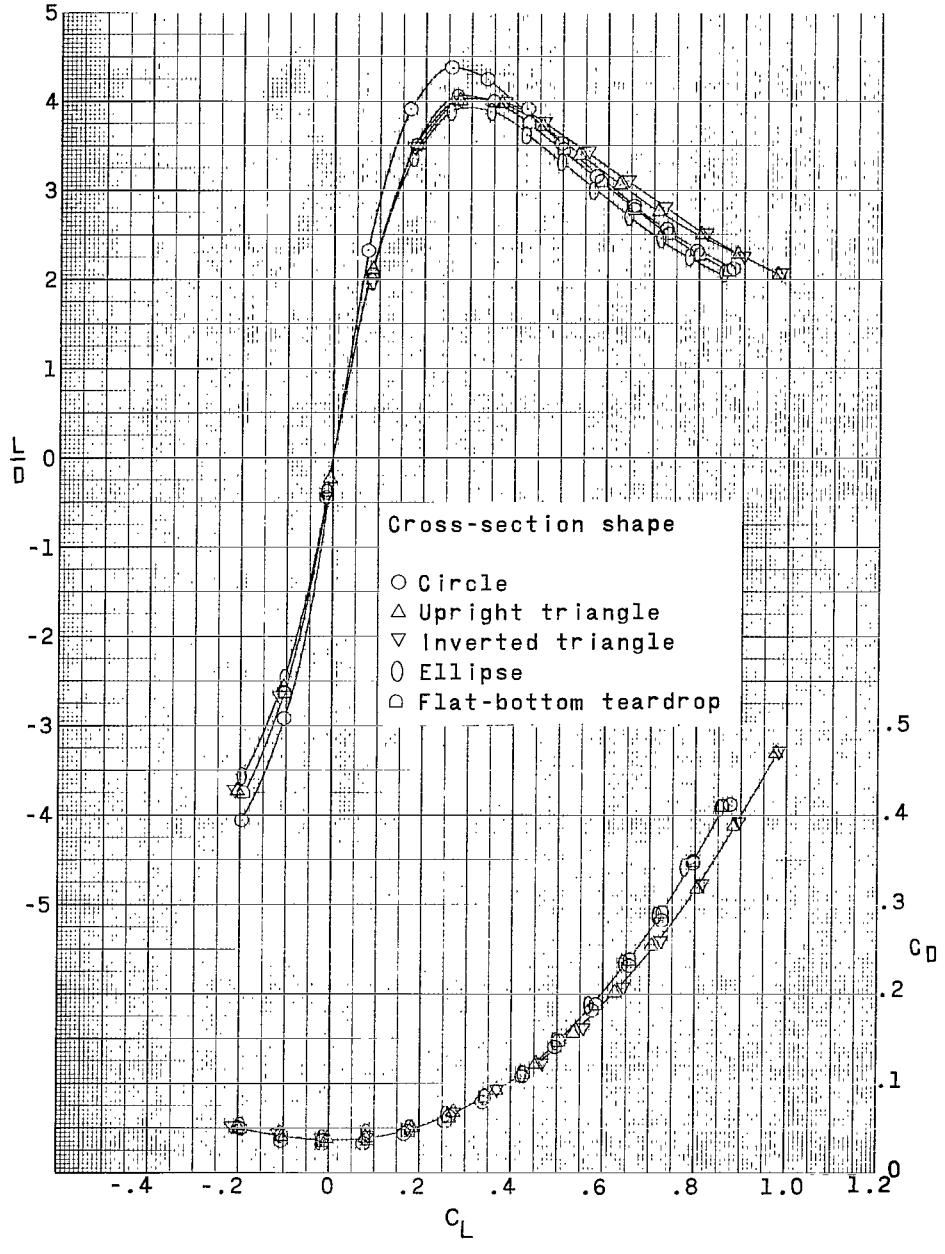

(a) M = 1.41.

Figure 11.- Effect of fuselage cross-sectional shape on aerodynamic characteristics in pitch.

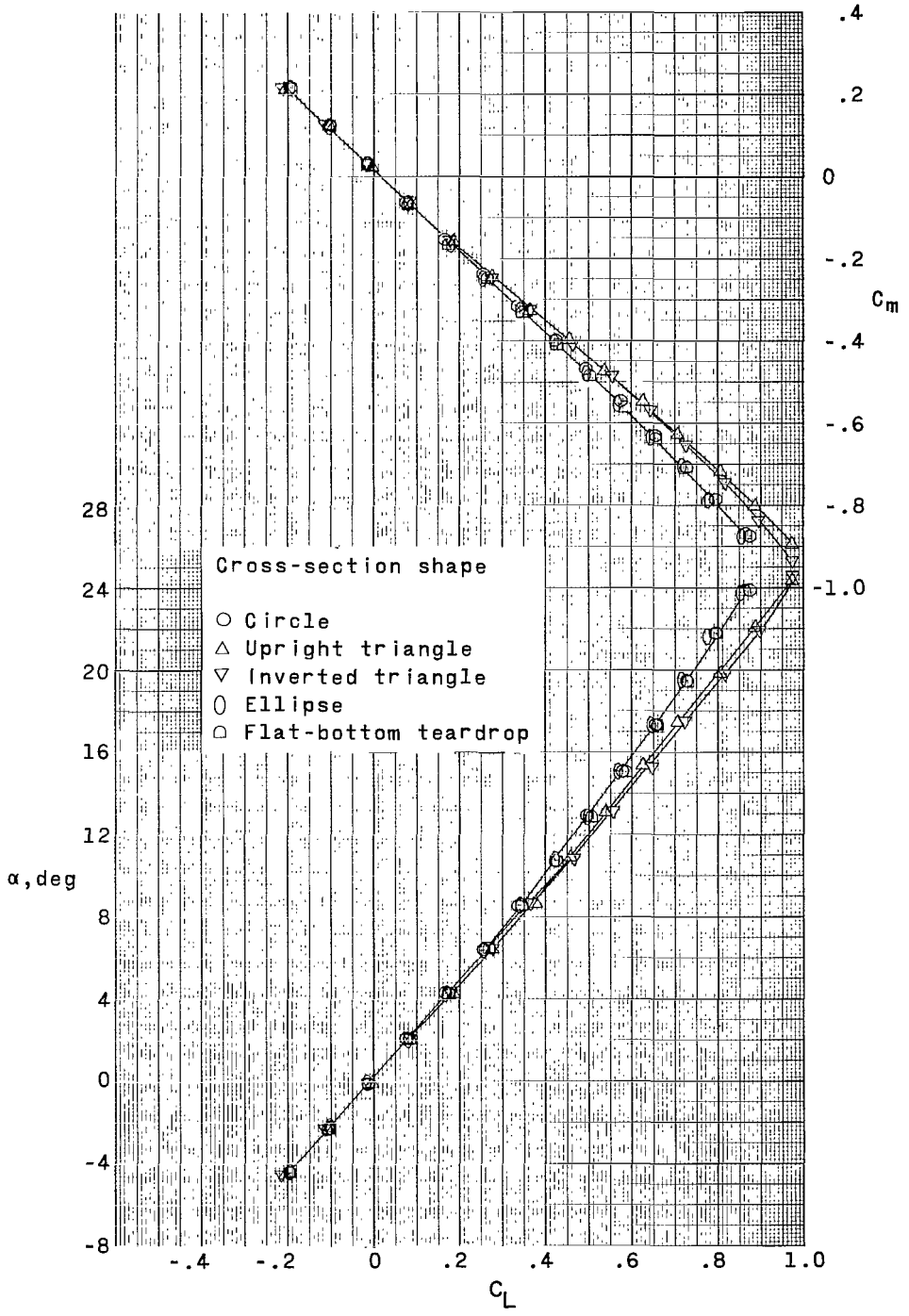

(a) Concluded.

Figure 11.- Continued.

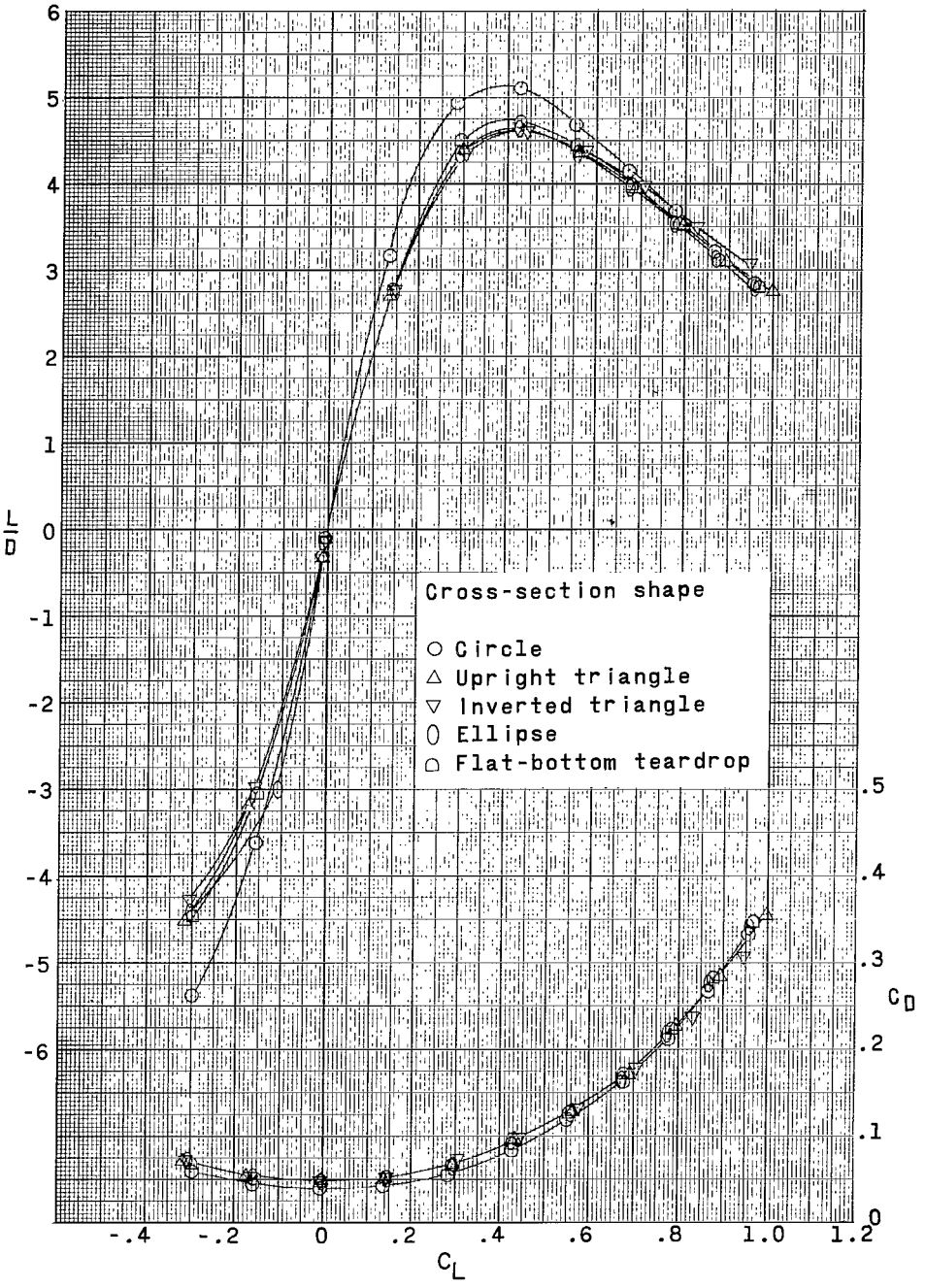

(b) M = 2.20.

Figure 11.- Continued.

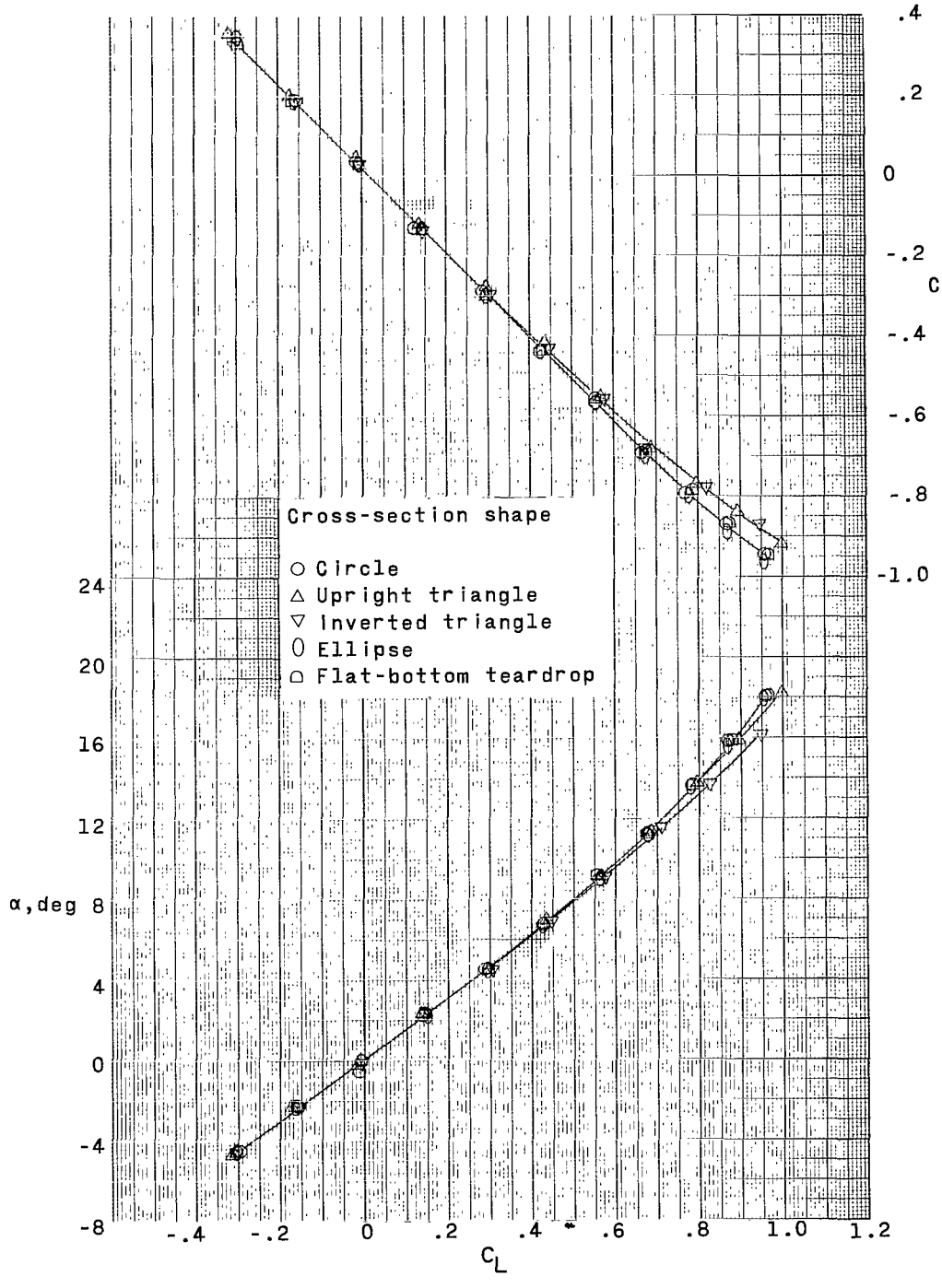

(b) Concluded.

Figure 11.- Concluded.

2/7/85

OR

"The aeronautical and space activities of the United States shall be conducted so as to contribute . . . to the expansion of human knowledge of phenomena in the atmosphere and space. The Administration shall provide for the widest practicable and appropriate dissemination of information concerning its activities and the results thereof."

—NATIONAL AERONAUTICS AND SPACE ACT OF 1958

NASA SCIENTIFIC AND TECHNICAL PUBLICATIONS

TECHNICAL REPORTS: Scientific and technical information considered important, complete, and a lasting contribution to existing knowledge.

TECHNICAL NOTES: Information less broad in scope but nevertheless of importance as a contribution to existing knowledge.

TECHNICAL MEMORANDUMS: Information receiving limited distribution because of preliminary data, security classification, or other reasons.

CONTRACTOR REPORTS: Technical information generated in connection with a NASA contract or grant and released under NASA auspices.

TECHNICAL TRANSLATIONS: Information published in a foreign language considered to merit NASA distribution in English.

TECHNICAL REPRINTS: Information derived from NASA activities and initially published in the form of journal articles.

SPECIAL PUBLICATIONS: Information derived from or of value to NASA activities but not necessarily reporting the results of individual NASA-programmed scientific efforts. Publications include conference proceedings, monographs, data compilations, handbooks, sourcebooks, and special bibliographies.

Details on the availability of these publications may be obtained from:

SCIENTIFIC AND TECHNICAL INFORMATION DIVISION

NATIONAL AERONAUTICS AND SPACE ADMINISTRATION

Washington, D.C. 20546